CHALMERS
UNIVERSITY OF TECHNOLOGY

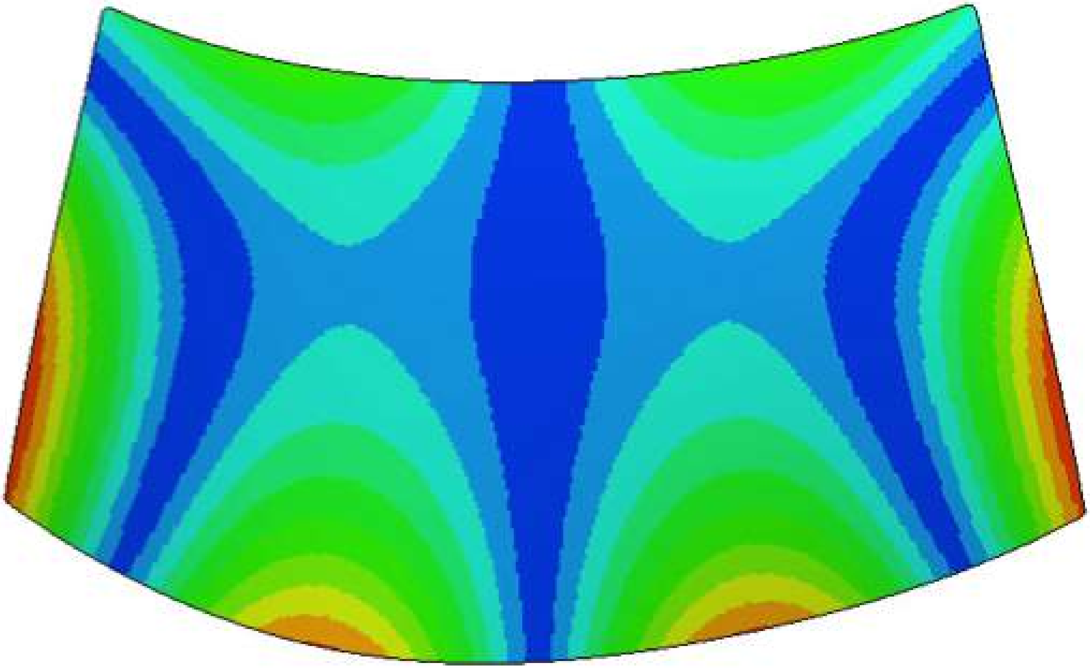

Method Development and Analysis of Tensile Stresses in Windscreens

A Study on the dynamic stresses on windscreens subjected to random vibrations

KARTHIK VASUDEVA MURTHY
PHILIP OLIVER REIS
Department of Industrial and Materials Science
Division of Material and Computational Mechanics
CHALMERS UNIVERSITY OF TECHNOLOGY
Gothenburg, Sweden 2018

Method Development and Analysis of Tensile Stresses in Windscreens

A study on the dynamic stresses on windscreens subjected to random vibrations.

KARTHIK VASUDEVA MURTHY

PHILIP OLIVER REIS

Department of Industrial and Materials Science
Division of Material and Computational Mechanics
Chalmers University of Technology
Göteborg, Sweden 2018

Method Development and Analysis of Tensile Stresses in Windscreens
- A study on the dynamic stresses on windscreens subjected to random vibrations.

KARTHIK VASUDEVA MURTHY, M.Sc Applied Mechanics
PHILIP OLIVER REIS, M.Sc Product Development and Materials Engineering

Supervisor: Eirini Chatzopoulou, Volvo Car Corporation, Torslanda, Sweden
Examiner: Ragnar Larsson, Department of Industrial and Materials Science

In co-operation with VOLVO CAR CORPORATION, Göteborg, Sweden
Department of Industrial and Materials Science
Division of Material and Computational Mechanics
Chalmers University of Technology
SE-412 96 Göteborg
Telephone +46 31 772 1000

Cover: Modal Response of the Windscreen.

Typeset in LaTeX
Chalmers Reproservice
Göteborg, Sweden 2018

Method Development and Analysis of Tensile Stresses in Windscreens
- A study on the dynamic stresses on windscreens subjected to random vibrations.

KARTHIK VASUDEVA MURTHY
PHILIP OLIVER REIS
Department of Industrial and Materials Science
Chalmers University of Technology

Abstract

The thesis work deals with the study and determination of static and dynamic stresses acting on windscreen structures during transportation from the manufacturing site to the production plant. To simulate the stress distribution, a finite element model is developed of the structure and tested. The evaluated results from the stress analysis are then verified against results from literature and by own experimental results. The constructed FE model is simulated for modal response, and the response is validated against data from the experimental modal analysis. The data from the experiment is also used to calibrate the material card in an effort to get the most realistic dynamic response.
The dynamic stress experiment was carried out at RISE Borås in accordance to ASTM D4169-16 DC3. Strain gauges were mounted at areas of interest. The readings obtained from the strain gauges used in the analytical calculation of stress, which were used to verify the finite element stress results. The fundamental aim of both experiments was to evaluate the dynamic behaviour and validate the numerical model. The pre-processing software ANSA was used to construct the finite element model and MSC Nastran was used as the FE- solver to simulate static and dynamic stresses on the structure. Transport loads were simulated using the random vibration load case, where a input load is in form of Power Spectral Density (PSD) data which describes the distribution of power into frequency components for a given time series. The input PSD was also in accordance with ASTM D4169-16 DC3, which is used to simulate the same response as in the experiment. During the numerical analysis, the glass and the intermediate PVB layer is assumed to be linear and isotropic. A validation of the numerical model was carried out against the experimental results to evaluate the predictive capability of the developed numerical model. The finite element model leads to good correlation of natural frequencies and their corresponding mode shapes at the lower range of frequencies valid till 100 Hz. This study is thus intended to construct and develop a FE model in order to predict the dynamic response and stress states experienced during transportation. It is further extended to predict the critical areas on the windscreen and help optimize the packaging of windscreens. During the course of study, it was found that, windscreens in the current transport arrangement experienced high stresses at areas close to the supports. The simulated stress values near the top right spacer (holding area) were close to the elastic limit of glass. This therefore, presented a high chance of damage to the windscreen when subjected to the random vibration.
Keywords: Dynamic Stresses, FE Method, Laminated Glass, Modal Analysis, Random Vibration, Windscreens, PSD

Acknowledgements

The authors want to acknowledge that this work was written in collaboration between two Universities, Karthik Vasudeva Murthy from Chalmers University from the Master of Science program in Applied Mechanics and Philip Oliver Reis from Jönköping University from the Master of Science program Product Development and Materials Engineering. The authors of this report were assigned together by Volvo Car Corporation, to complete this research work.
The authors would like to take this opportunity to express their gratitude to Professor Lennart Mähler, Jönköping University and Professor Ragnar Larsson, Chalmers University for their guidance and supervision during the course of study.
The authors also would like to thank their supervisor at Volvo Car Corporation Eirini Chatzopoulou and Jonas Ask for all their assistance in the fruitful completion of the study. Furthermore, the authors would like to thank everyone from the Exterior Glass Group at Volvo Car Corporation for their hospitality during these weeks of study and in making the stay at Volvo Car Corporation enjoyable. Finally the authors would like to thank their families and friends for their all support and kind words during the thesis study.

Karthik Vasudeva Murthy, Philip Oliver Reis
Gothenburg, September 2018

Contents

Abbreviations

DOF - Degree of Freedom

EMA - Experimental Modal Analysis

FRF - Frequency Response Function

FE - Finite Element

FEM- Finite Element Method

NVH - Noise Vibration and Harshness

MOOF - Multiple Degree of Freedom

PSD - Power Spectral Density

RBE - Rigid Body Element [37]

RMS - Root Mean Square

SDOF - Single Degree of Freedom

SPC - Single Point Constraint [37]

VCC - Volvo Car Corporation

Hz- Hertz

MPa- Mega Pascals

Nomenclature

ζ - damping constant

ω_n- Natural Frequency

k- Stiffness constant

F- Applied external force

M- Mass of the body

ω_d- Damped Frequency

C_c- Critical Damping

P- Probability of Gaussian Distribution

E- Young's Modulus

ν- Possion's Ratio

$\epsilon_a, \epsilon_b, \epsilon_c$- Strain Measurements in local coordinates (a,b,c)

σ_{max}- Maximum Principal Stress

1

Introduction

1.1 Background

Volvo Car Corporation (VCC) is an automotive manufacturer with Swedish roots headquartered in Torslanda, Gothenburg [1]. The first Volvo car rolled off the factory's production line 1927, ever since then VCC have established themselves as one of the most influential and well-recognized cars brands in the world. As of 2010, VCC is a part of the Zhejiang Geely Holding of China, with the ambition of producing quality cars within safety technologies, electrification and autonomous drive. This master thesis will be taking place at the department of exterior glass in Torslanda, Gothenburg.

With the advancement of autonomous driving solutions, passenger safety and crash worthiness, windscreens play a vital role in the development of automobile structures. To that effect, the windscreens are constructed as a sandwiched glass-plastic structure. The plastic at the centre is typically soft polymer such as PolyVinyl Butyral (PVB). The reason behind using laminated glass is that it offers better crash protection wherein, the plastic mid-layer holds the glass structure from shattering which in turn reduces injuries such as cuts by glass fragments. Windscreens play a vital role in the development of automotive structures, high quality is a requirement for both aesthetics and functionality [28].

The windscreens are stacked in racks by the supplier, see figure 1.1 and then transported using trucks from the production plant to the assembly plant. Glass is generally a brittle material which is to be handled carefully to avoid any damage and being transported for long distances should endure the vibrations generated due to the movement of the truck [27]. Moreover, the vibrations are random and are dependent on various parameters such as roughness of roads, the suspension of trucks, packaging orientation to name a few. Hence, it becomes vital to understand how the vibrations affect the windscreen and to that effect, this thesis deals with the study of dynamic responses of the windscreen and the determination of stresses in the windscreens when they are subjected to transportation loads [5]. Thus, this thesis work was proposed to gain better understanding of the effect of dynamic loads on windscreens during transportation.

Figure 1.1: Stacking of windscreens

1.2 Purpose

The objective of this master thesis is to develop a numerical FE model in order to simulate and predict the stresses in windscreens when it is exposed to transportation loads. As transportation loads are dynamic in nature a major portion of the study is dedicated to understanding the dynamic behaviour of laminated windscreens.

1.3 Hypothesis and Research Question

The following hypothesis and the research questions have been formulated to identify difficulties and establish knowledge of research:

1.3.1 Hypothesis

During transportation. The stacked windscreens will experience random vibration due to shifting road conditions. This may lead to high forces and loads acting on the structure and induce tensile stresses on the surface of the windscreens.

1.3.2 Research Questions

- What are the natural frequencies of vibration of the windscreen structure?
- How does the material parameters change the lamina characteristic?

- What is the influence of material properties on the dynamic behaviour of the structure?
- What is the structure's stress state achieved during random excitation?
- How could the current packaging affect the stress distribution during random vibration?
- How could resonance produce a potential failure for windscreens?

1.4 Limitations

As this is a research project, it has some necessary limitations:

- During the construction of the FE model of the windscreen, the contact between the plastic holders and the glass surface is modelled using rigid body elements (RBE3) in order to simplify the model [37].
- As exact numerical values for static loads acting on the windscreen were unavailable, the load was calculated by making assumptions to the angle of tilt of the stacked windscreen, which may lead to conservative results i.e. the predicted stresses may be higher than reality.
- Glass and PVB are both considered exhibiting linear elastic behaviour.
- Random vibration loads are simulated using input Power Spectral Density (PSD) in accordance with ASTM D4169-16 DC3, see appendix C
- During the random vibration experiment, input loads were limited to 30Hz due to limitations of the shaker rig
- As the strain gauges mounted during the vibration test can only give strain readings on the top surface of the windscreen, the variation of strain and stress through the along the thickness of the windscreen cannot be validated with experimental data.
- Due to the assumption of linear isotropic behavior of both glass and PVB, the stress is also assumed to vary linearly through the thickness of the windscreen, see figure 2.1.

1.5 Thesis Outline

The thesis is structured into several chapters, a brief outline of each chapter is presented here.

- Chapter 2: Narrate the theoretical background of relevant literature within the field of material knowledge, structural vibrations, signal processing and finite element method
- Chapter 3: Narrate the methodology selection of the investigation with techniques and tools used in the search referred to the theoretical background
- Chapter 4: Narrate the results from the methodology from Chapter 3
- Chapter 5: Summarizing the results and methodology with conclusion and discussions of the findings. Recommendations for continued work or future findings are also stated in this chapter.

2
Theoretical background

The following chapter contains all relevant theoretical literature, which forms the basis for the outlined methodology of this master thesis. We start this chapter with an introduction to the structure of the windscreen and explain the theory behind laminated glass. This is followed by an introduction to structural vibrations and resonance. A brief theory on modal analysis is presented followed by a review of random vibration load case with a introduction to PSD analysis and its application. Finally, the chapter ends with an overview on the theory behind finite elements and its implementation with respect to this thesis work.

2.1 Laminated Glass

Laminated Glass (LG) in automotive structures consists of two sheets of glass bonded by a plastic interlayer. The most commonly used interlayer is PVB. LG is more desirable in automotive applications due as its enhanced safety, security, fire-resistant and sound attenuating properties. One of the most important properties of laminated glass is its ability to retain its structural composure when exposed to high impact loads. When LG is subjected to impacts as the glass breaks it is held together by the plastic interlayer which prevents the glass from shattering and forming sharp edges[27].
The lamination of windscreen glass with the plastic interlayer takes place at around 140^{o}C. The process takes place in a pressure vessel called autoclave [27].
The windscreen structure for the assigned windscreens are made up in three layers; the top layer of glass has a thickness of 2.1 mm with the bottom layer having a thickness of 1.6mm. The interlayer PVB has a thickness of 0.76mm. Therefore, the effective thickness of the laminated windscreen glass is 4.46mm [27], [3].

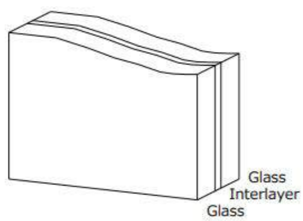

Figure 2.1: Laminated glass- Sandwich structure [27]

Compressive Strength	880-930 MPa
Tensile Strength	30-90 MPa
Young's Modulus	70-75 GPa
Possion's Ratio	0.2-0.3

Table 2.1: Mechanical Properties of Glass[27]

Tensile Strength	≥20 MPa
Shear Modulus	0-4 GPa
Possion's Ratio	0.45-0.49

Table 2.2: Mechanical Properties of PVB[27]

The material properties of glass and PVB are given in table 2.1 and table 2.2 respectively.
The tables describe both glass and PVB to have a range of values for Young's modulus and Possion's ratio which can be attributed to the laminate being manufactured by different processes. Hence it becomes vital to establish a material card with the most appropriate values in order to obtain the most accurate representation of the reality. With the proposed methodology, the material data which provided the best representation of reality is shown in section 4 and its Nastran material card is shown in appendix E.

2.2 Modal Analysis - Experiment

Modal analysis is the study of dynamic properties of a system in the frequency domain. It gives us an overview on the limits of the response of the system [6]. The various parameters that characterize the output of modal analysis are mode shapes and the eigen frequencies associated with those mode shapes [26]. The excitation of these eigen frequencies is carried out with no specific boundary conditions or in the Free-Free state so, the only factors influencing the dynamic behaviour of the structure will be its inherent mechanical properties.

2.2.1 Mode and Mode Shapes

A mode is defined as a combination of deformed shape in which the structure exchanges kinetic and strain energies continuously. Therefore, a point on a body that moves, will at un-deformed positioning have maximum speed and thus the maximum kinetic energy, while at the maximum deformed position have the lowest kinetic energy.
The frequency at which of each of these modes occur indicate the natural frequency of the system. A given body can have infinite number of natural frequencies and when loads are applied at these frequencies, the energy induced will cause an additional increase in the motion of the structure at that mode[6].

2.2.2 Frequency Response Function

Frequency response function (FRF) is a quantitative measurement of the output of a structure in response to a excitation load which leads to the identification of dynamic resonant frequencies and describing the mechanical properties of a component [26][9]. The FRF plot figure 2.2, shows the linear time-invariant system frequency domain relationship between the input (x) and output (y) from a preformed experiment.

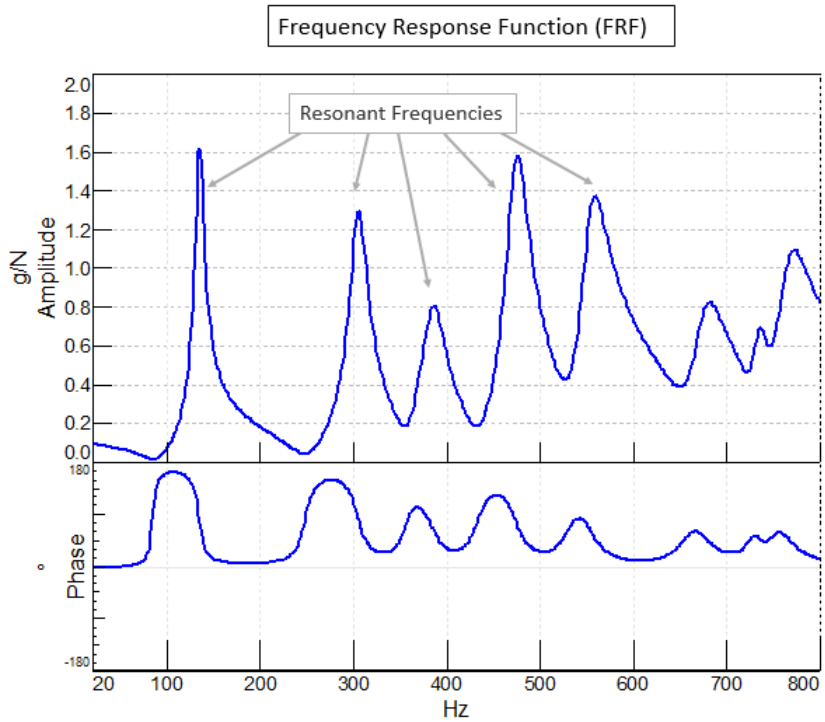

Figure 2.2: Amplitude and Frequency phase of FRF [9]

2.2.3 Excitation

Excitation having sufficient magnitude and frequency bandwidth is applied through various input methods, the most common being Impact hammer or an electrodynamics shaker [26].

2.2.3.1 Impact Hammer Excitation

When exciting a body using an impact hammer short term impacts are generated at selected points through-out the body of the component. Impact hammers have the capacity to excite a wide range of frequencies of the body and are most commonly used due to its flexibility and ease of operation [26]. Impact excitation produces a transient signal with the bandwidth of the frequency being determined by the stiffness of the hammer and the structure. The range of these excitation is dependent on the tip material of the hammer [26].
One of the drawbacks of impact testing is the increased crest factor, which decreases

the signal to noise ratio and may impart some non- linear behaviour to the system [26].
There is also an influence of human error on the calculated output as each excitation is imparted by hand of a human which may vary from excitation to excitation. So utmost care is to be taken to see that there is good coherence between consecutive impacts[26]. During the course of this work, Impact hammer excitation is preferred due to its flexibility and good excitation of eigen frequencies at a lower bandwidth of around 1-100Hz.
Shakers on the other hand have a preprogramed uniform impulse force than the impact hammer and are usually used for Multi-Input Multi-Output analysis with the test setup is more complex.

2.2.3.2 Coherence in modal analysis

As stated earlier to get a good output in impact testing, it is vital to have good coherence between consecutive hits. Equation 2.1 defines a coherence function, where D_{xx} and D_{yy} are the auto spectral densities and D_{xy} is the Fourier transform of the Fourier transform of the cross-correlation function between two functions.

$$C_{xy} = \frac{\mid D_{xy} \mid^2}{D_{xx} D_{yy}} \tag{2.1}$$

In ideal cases, coherence function is equal to unity but, it practice it not possible to avoid incoherence which can be attributed to the existence of anti- resonance [26].
During the course of this study, the software Siemens LMS TestLab, is used as the post processing tool, where the coherence is taken as an average of several hits to smooth out the curve.

2.3 Equation of Motion

To describe the structural dynamic the best representation is a Single-Degree-of-Freedom (SDOF)-system. A SDOF-system is a simplified description of a system, which can be illustrate with a mass attached with a spring and a damper with a motion along a translational axis [7]. Figure. 2.3 represents an oscillator concept model consisting of a frictionless mass, m, acting by a dynamic force, $F(t)$, which is attached to a massless spring with a stiffness, k, and massless viscous damper, c.

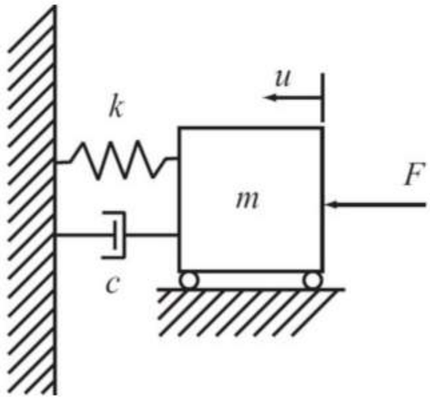

Figure 2.3: The oscillator concept of a SDOF system

To derive the equation of motion is essential to start with Newton's second law of motion, equation 2.2, which states that the acceleration of an object is dependent upon two variables - the net force acting upon the object and the mass of the object, which can be represented as.

$$\sum F = m\ddot{x} \tag{2.2}$$

When Newton's second law is applied to the mass-damper system the spring and the damper act as parallel time derivative counter forces to the applied dynamic force, where 'k' which represents the stiffness of the spring is proportional to the displacement and the damping coefficient 'c' is proportional to the velocity of the system, $\dot{x}$.The equation motion for the structure can be rewritten as equation 2.3.

$$F(t) = m\ddot{x}(t) + c\dot{x}(t) + kx(t) \tag{2.3}$$

However, structures are not always adequate to be represented as a SDOF-system, most structures are composed with multiple degrees-of-freedom, which puts the SDOF simplification of the system at the risk of yielding erroneous frequency and mode shapes. In order to describe a real-life structure, a Multi-Degree-of-Freedom (MDOF) system is used to represent the system more accurately. The principle of a MDOF-system is similar to a SDOF-system, with the only exception being that the mass, spring and dampers are expressed in the form of symmetric matrices of order $[NxN]$ and column vectors as N, where 'N' is defined by the degrees of freedom. The compact equation of motion for a MDOF-system thus results in equation 2.4.

$$\Big\{F(t)\Big\} = \Big[M\Big]\Big\{\ddot{x}\Big\}(t) + \Big[C\Big]\Big\{\dot{x}\Big\}(t) + \Big[K\Big]\Big\{x\Big\}(t) \tag{2.4}$$

Equation 2.4 is an overview of a diagonal mass matrix structure with respect up to 'N' degree-of-freedom wherein, the mass, damping and stiffness of the system are the matrix coefficients, while external force, displacement, velocity and acceleration are represented as vectors.
The constituents of equation [2.4] are explicitly stated in equations 2.4 to 2.8.

$$\Big[M\Big] = \begin{bmatrix} m_1 & \cdots & 0 \\ \vdots & \ddots & \vdots \\ 0 & \cdots & m_n \end{bmatrix} \tag{2.5}$$

$$\begin{bmatrix} C \end{bmatrix} = \begin{bmatrix} c_1 + c_2 & -c_2 & \cdots & 0 \\ -c_2 & c_2 + c_3 & \ddots & \vdots \\ \vdots & \ddots & \ddots & -c_N \\ 0 & 0 & -c_N & c_{N-1} + c_N \end{bmatrix} \tag{2.6}$$

$$\begin{bmatrix} K \end{bmatrix} = \begin{bmatrix} k_1 + k_2 & -k_2 & \cdots & 0 \\ -k_2 & k_2 + k_3 & \ddots & \vdots \\ \vdots & \ddots & \ddots & -k_N \\ 0 & 0 & -k_N & k_{N-1} + k_N \end{bmatrix} \tag{2.7}$$

$$\begin{Bmatrix} F \end{Bmatrix} = \begin{Bmatrix} F_1 \\ F_2 \\ \vdots \\ F_N \end{Bmatrix} \begin{Bmatrix} x \end{Bmatrix} = \begin{Bmatrix} x_1 \\ x_2 \\ \vdots \\ x_N \end{Bmatrix} \begin{Bmatrix} \dot{x} \end{Bmatrix} = \begin{Bmatrix} \dot{x}_1 \\ \dot{x}_2 \\ \vdots \\ \dot{x}_N \end{Bmatrix} \begin{Bmatrix} \ddot{x} \end{Bmatrix} = \begin{Bmatrix} \ddot{x}_1 \\ \ddot{x}_2 \\ \vdots \\ \ddot{x}_N \end{Bmatrix} \tag{2.8}$$

Solving the MDOF equation of motion analytically as the structures become complex with intricate boundary conditions can be challenging. To eliminate that risk, numerical models of the geometry with properties are implemented and processed in a finite element environment.

2.3.1 Measurement of FRF

FRFs are calculated at each user defined point on the component structure by taking the ratio of output response to input excitation. The instantaneous time domain data from the input and output is transformed into frequency domain data using Fourier transforms [26]. In the case of this study, the FRF corresponding to acceleration are measured at user defined positions and is defined by the equation 2.9, where ζ is the damping ratio, ω_n is the natural frequency of the system, 'k' is the stiffness of the body and 'F' is the external applied force.

$$\frac{d^2x}{dt^2} + 2\zeta\omega_n\frac{dx}{dt} + {\omega_n}^2 x = \frac{\omega_n^2 F}{k} \tag{2.9}$$

The acceleration function is thus given by,

$$H(\omega) = \frac{\ddot{x}(\omega)}{F(\omega)} = \frac{1}{k}\frac{-\omega^2\omega_n^2}{\omega_n^2 - \omega^2 + j(2\zeta\omega\omega_n)} \tag{2.10}$$

The magnitude of this complex function is given by,

$$\mid \frac{\ddot{x}(\omega)}{F(\omega)} \mid = \frac{1}{k}\frac{-\omega^2\omega_n^2}{\sqrt{(\omega_n^2 - \omega^2)^2 + (2\zeta\omega\omega_n)^2}} \tag{2.11}$$

2.3.2 Natural Frequency and Damping

When a mass undergoes a vibration motion, its static equilibrium state begins to deform in the form of a simple harmonic motion [8]. Natural frequency is the rate at, which an object vibrates when there are no external forces acting on it. Analytically, the natural frequency is denoted by ω_n. In the case of damped vibrations ω_d, is given by equation [2.12] where, ζ denotes defines the damping coefficient.

$$\omega_d = \sqrt{1 - \zeta^2 \cdot} \omega_n \tag{2.12}$$

Damping is a process of diminishing exposed vibrations or motions over time until the structure reaches equilibrium. When motion is induced in a structure, energy is formed in terms of kinetic a strain energy, which is dissipated by both internal friction and various contact mechanisms simultaneously [8]. In the case of the windscreens being transported, the damping may occur due to the friction between the windscreens and the supports in its holding position.
However, as these damping mechanisms are complex it becomes complicated to describe the phenomenon mathematically. Therefore, a damped system is idealized for a free linear viscous damping SDOF system.
For a damped system, the damping coefficient is the ratio of actual damping to critical damping see equation 2.13.

$$\zeta = \frac{c}{c_c} = \frac{c}{2 \cdot \sqrt{km}} \tag{2.13}$$

For a undamped system, the natural frequency ω_n is given by equation 2.14.

$$\omega_n = \sqrt{\frac{k}{m}} \tag{2.14}$$

Combining equations [2.13] and [2.14], arrive according to equation 2.15 at.

$$c_c = 2m\sqrt{\frac{k}{m}} = 2m\omega_n \tag{2.15}$$

For an undamped system, the time to complete one cycle can be denoted as the natural period which is given by equation 2.16.

$$T_n = \frac{2\pi}{\omega_n} \tag{2.16}$$

Frequency which is defined as the reciprocal of the time period is given by equation 2.17.

$$f_n = \frac{1}{T_n} \tag{2.17}$$

Therefore, the natural frequency of the undamped system f_n is given by equation 2.18.

$$f_n = \frac{\omega_n}{2\pi} \tag{2.18}$$

It is clear from equation[2.18], that the natural frequency of vibration of a undamped system is a function of mass and stiffness of the system.

2.4 Introduction to Random Vibration

In the automotive industry, car structures are generally combinations of fastened parts, which together form a supporting framework of the cars. Cars always run a risk of being exposed to unwanted dynamic loads during their operation sources. This is also true in the case of a truck, which is transporting any packages. These unwanted dynamic loads or vibrations can be classified into two types, deterministic which is caused due to the rotating parts within the vehicle and the other being un-deterministic or random vibrations where the loads can be unpredictable and are influenced by factors such as road roughness. As these vibrations tend to be random, its effect on the system cannot be precisely predicted [25].
Before starting simulating random vibrations, it is important to have a clear understanding about the theory behind. For this to be accomplished, it is fundamental to have a basic knowledge about random vibrations when a system is suspected of being exposed to failure due to fatigue, resonance or vibration excessive from other components.
The introduction to this chapter begins with the theory and equations governing structural vibrations when a body is subjected to dynamic loading. It discusses about the equation of motion describing the phenomenon, where the structure tends to vibrate or oscillate at specific frequencies, which are termed as natural frequencies of the system.

2.4.1 Random Vibration Analysis

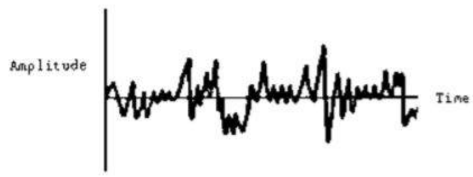

Figure 2.4: Amplitude-Time history of random vibrations [5]

Random vibration in its true sense should not be considered to having no specific patterns as it becomes impossible to define a vibration setup, which is totally unpredictable. So the transport load case is treated to be under a special category of stationary random vibrations[5].
The stationary case can be explained as in that the factors that influence the random vibration load set do not change significantly over a period of time so that its application will yield the same results when applied at different times and will have a certain amount of repeatability to its application [5].
Applying this to our case of transportation of windscreens, the stationary random load has the same Root Mean Square (RMS) amplitude remains constant with time. Random vibrations do not possess any absolute value at any given point [5]. When a body is subjected to such random vibration loads, it experiences numerous frequencies being excited at the same time which increases the possibility of many

components experiencing structural resonance simultaneously[5]. As random vibrations cannot be expressed mathematically as an exact function of time, statistical approaches are used to determine the probability of occurrence of a particular amplitude [5].
To be treated as a stationary case, possible time histories of amplitudes measured in the frequency range of excitation are to be generated. By using this parametric data, random analysis is analyzed in the statistical sense[5][23].

2.4.1.1 Power Spectral Density

PSD is the most common way used to define random vibrations. PSD usually defines the distribution of power over a certain frequency range. Numerically, it is the mean square value of magnitudes passed by a certain filter, divided by the bandwidth of the filter[5][23].
In actual practice, the generated PSD data is obtained by averaging the amplitude of the random process using a statistical method. The most common method used to determine the probability of occurrence of particular amplitudes is Normal or Gaussian distribution [23][5], which is defined by the equation 2.19.

$$P = \frac{1}{\sqrt{2 * \pi}} e^{[(\frac{-1}{2})[(\frac{x}{x_{rms}})]^2]} \tag{2.19}$$

Equation 2.19, when plotted results in figure 2.5 with the Y- axis representing the ratio of instantaneous value with the Y- axis representing the RMS values of any parameters such as displacement, velocity or acceleration [5].

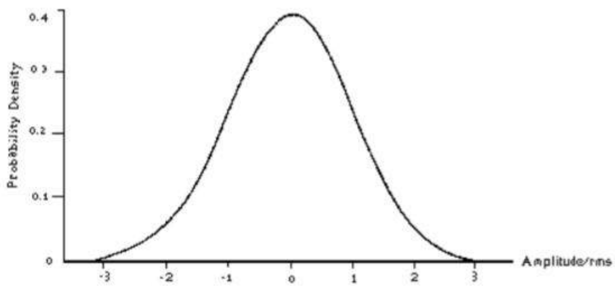

Figure 2.5: Gaussian Distribution [5]

Random vibrations in the time domain are not very useful and not much information can be accessed by it, so Fourier transforms are used to transform this time domain data into useful frequency domain data which helps in identifying the different amplitude for different frequency components in the signal [23].
With respect to the work carried out in this thesis, the PSD data is generated as per the standard ASTM 4169-16 DC3 [19] and used as input to both the experimental test rig and the finite element simulations.

2.5 Mechanical Resonance

Mechanical resonance is a phenomenon when, in which a forced motion induced at a frequency that coincides with the structure's eigenfrequency can cause motion amplitude of the structure that is greater than the force motion amplitude [10].
In other words, if the induced frequency corresponds to the natural frequency of the system, it causes an increase of energy leading to uncontrolled vibrations. In a undamped system, if the load is applied at natural frequencies the deformation amplitude can grow to infinity. Thus, structures and components have damping present in the system to eliminate the chance of large resonant frequency response. However, if a forcing frequency is constantly present it can cause failure and cracking as the deformation continues.
A notorious event of the effects of resonance was when the Tacoma Narrows Bridge, Washington state USA year 1940, collapsed after the structure oscillations there a picture of the bridge in motion is visualized in figure 2.6 [10].

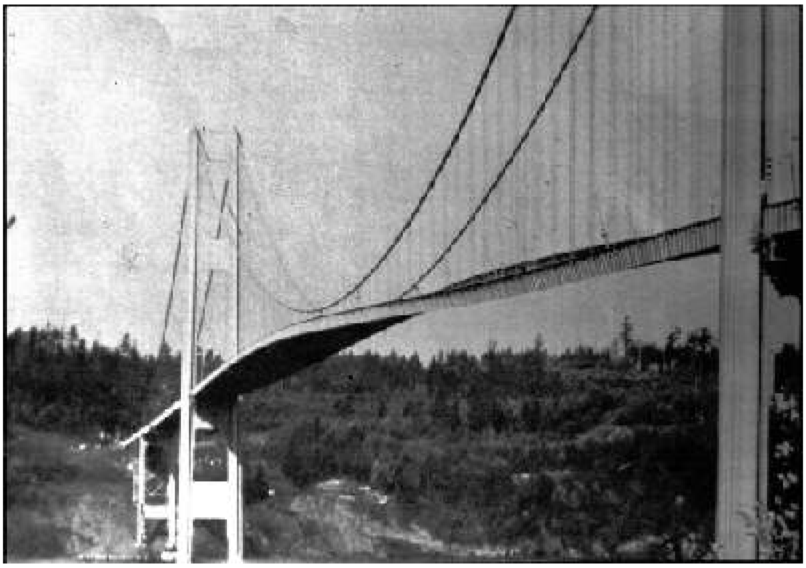

Figure 2.6: A photo of the Tacoma Narrows Bridge deformation cause of resonance [10]

2.6 Signal Processing

A signal is defined as a function of information about a system's behavior or attributes of some phenomenon varies over time or in space [11]. A wave powers modern communication (speaking or music), the conveying temperature information from a thermocouple or an electromagnetic wave conveying reaction information from accelerometers at structures or human bodies.
Thus, Signal processing is basically an operating activity (manipulation) of an input signal, to produce an output signal. However, sampling a signal can cause error in the way it is being sampled. Here is a clarification procedure stated of how to lower the potential risk of conveying sampling errors.

2.6.1 Aliasing

Aliasing is an inappropriate or an undesired sampling phenomenon with the potential to sample erroneous input signals to a sampling data system. The phenomenon occur when sampling a signal at an inappropriate sampling rate, a high frequency signal may appear as a low frequency rate due to the inappropriate sampling rate of the signal [12]. Enables the risk of recording a different input signal. Figure 2.7 illustrates a temperature signal sampling there the problem of aliasing is addressed if a signal is sampled with the same rate for each period. The rate outputs a new signal, which does not corresponds with the initial input signal.

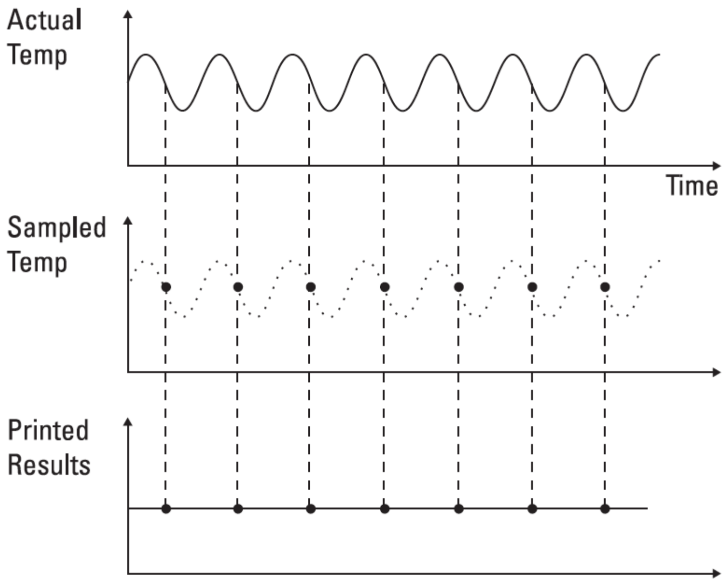

Figure 2.7: A poor sampling rate example illustrated by a given signal, sampling signal and alias signal [12]

By establishing a new sampling rate, the aliasing phenomenon can be avoiding. The Nyqvist sampling theorem, also called Nyqvist Frequency (equation 2.20), is a nominal sampling interval for zero to the highest frequency given at signal [13]. The theorem is expressed in mathematical terms, which is explained as the sampling frequency should at least be the twice of the highest frequency of a signal to avoid aliasing.

$$f_s \geq 2f_{max} \tag{2.20}$$

$$\Delta t = \frac{1}{2f_{max}} \tag{2.21}$$

For equation 2.20, f_{max} express the highest frequency signal of a period and f_s is the sampling frequency. If a signal has greater frequency than the half of the sampling frequency, the signal would be read as a lower frequency and f_s will alias. Equation

2.21 expresses the sampling interval, Δt, and with the sampling frequency. To clarify the mathematical term a sampling problem will be example: If the maximum desired sampling frequency is 300 Hz then the sampling frequency should at least be up to 600 Hz and a sampling interval of 1. 67 ms according to theorem.

With Nyqvist sampling theorem it is possible to identify the distance between the peaks of a wave within a solid material by the wavelength equation 2.22. Here λ is the wavelength of the signal measured from two points in the same phase is equal to the sum of the speed of light c of a substance divided by its frequency [14].

$$\lambda = \frac{c}{f} \tag{2.22}$$

A new equation can be formulated for identifying a secure measurement distance for the wave signal and minimizing the erroneous of aliasing.

2.7 Finite Element Method

Finite Element Method (FEM) is numerical solution method suitable for solving and simulating complex physical states in a virtual environment. A FE-analysis primarily consists of stages starting with the discretization of structure where, the element types, material parameters and the mesh are defined. This is followed by the application of the boundary conditions, which accurately simulate the environment surrounding the structure. The model is then run using a commercial finite element code, which solves the simulation and a post processor is then used to view the generated results [15]. During meshing, the body or structure is broken down into multiple elements, FEs, which is equivalent over the system. To sustain a good connection over the geometry, the FEM-units are connected with points also referred as nodes. The nodes are functioning as connectors or glue between two or more units with boundary lines.[26] The main advantage of FEM is achieved when calculating complex geometries or loadings, which is a challenge if not impossible to obtain by analytical mathematical solutions. As part of this thesis work, the pre-processing was carried out in ANSA [35], with the modal and random vibration simulation carried in the NASTRAN environment [37] and the post processing was carried out in META [36].
As numerical modeling provides advantages with regards to working efficiency, this is also coupled with the method helping with virtual testing which bring down the frequency of experimental analysis. These numerical models are constructed such that they represent the reality most accurately. As experimental testing is a cumbersome and costly to process, virtual testing and simulations provide a more economical and efficient process to achieve good results.

2.7.1 Elements, Node and Shape Function

As stated earlier, the structure or body is divided into multiple elements and meshing is carried out using the pre-processing software. The user's judgment concerning the mesh size and element type to be used is dependent on what is desired level on accuracy required form the simulation. Sizing the mesh is vital enough to output a usable result, having a smaller mesh size increases the computational time and storage space required, but yields a more realistic result [15]. Hence, the user performing FE simulations always performs a fine balance between computational time and accuracy of the solution [18]. Elements in FEM define the degrees of freedom (DOF) of a node. These are built in either one-, two-, or three-dimensions, each dimension giving more accurate simulation of the structure and are used depending of what is of interest.

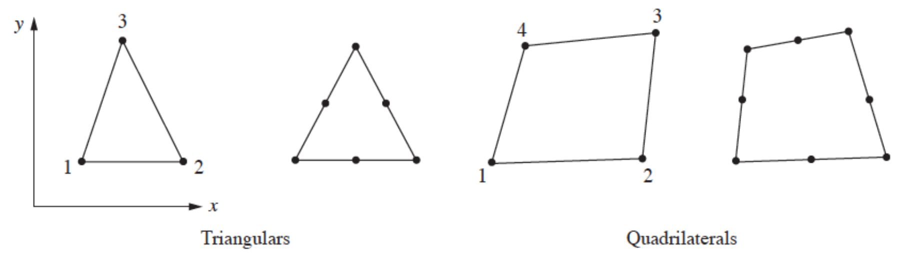

Figure 2.8: Shell element construction [15]

Two-dimensional (2D) or shell elements are constructed linearly between the nodes and results in simple triangular or quadrilateral element [15], Figure 2.8. These elements are used to predict deformation and stress in plane. A 2D shell element mathematical simplification of solid elements, and has the advantage of reducing computing time and convergence errors.

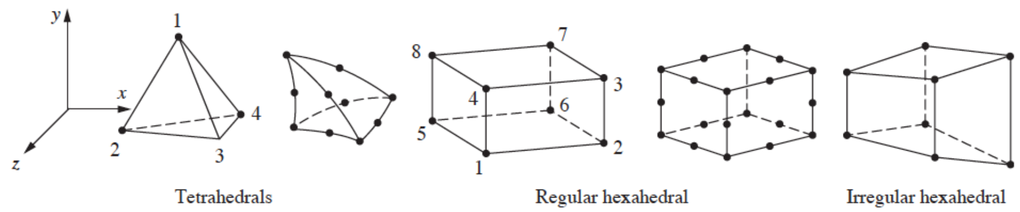

Figure 2.9: Solid element construction [15]

Three-dimensional (3D) or solid elements are generally tetrahedral and hexahedral in construction [15], Figure 2.9. These elements are used as a more accurate representation of the any structure with ability to predict out of plane displacements and stress fields. This accuracy comes at the cost of computational time and storage space.

With 2D or 3D elements, the FE approach works by approximating the shape of the structure with a finite number of discretized segments generated after meshing the structure. Each node has several DOFs which are solved with the help of differential equations. A shape function is used to interpolate the computed values such that they can be shape function can be represented in the form of a polynomial function [26].
During the course of this work, FE models are constructed using 2D Shell elements

and 3D hexahedral elements. In the case of 2D Shell elements, 4 noded quad elements are used in construction. The elements have 5 DOFs accounting to 3 translations and 2 rotational DOFs. These elements possess the capability to predict in plane tensile and compressive stresses. With the elements being 2D the stress through the thickness cannot be predicted. The elements are constructed using plane stress assumptions but this restricts the load application to only in plane loading.
As the laminate consists of a sandwich layer of PVB between layers of glass, it becomes vital to understand the distribution of stress through the thickness of the laminate. Thus, the FE model is also constructed using 3D hexahedral elements. These elements are typically 8 noded and possess 3 DOFs. As these elements have prescribed thickness they form a 3D solid mesh and thus can predict out of plane stresses. During the course of this work, 3D elements are used in the construction of the windscreen laminate structure. As the 3D mesh representation of the structure is true to reality [18], the results from these simulations are used in the current methodology to validate and calibrate the stress outputs from the 2D shell modeling

3

Method and Implementation

This chapter gives a detailed description on the methodology used in the course of this study to achieve the set objectives. Initially a narrative outline is presented and followed up with a deeper insight into the various phases of work carried out. The proposed methodology forms the basis of the results presented in chapter 4 and further discussed in chapter 5. During the course of this method, two windscreens are used as specimens and are termed as Windscreen A and Windscreen B. The major difference between the two windscreens is the geometrical dimensions with windscreen A being comparatively larger than windscreen B. The laminate structure however remain the same as discussed in Section 2.1
In order to accomplish the objective 1.2, the methodology is divided into two phases,

- Modal Analysis
  - Numerical Modal Analysis
  - Experimental Modal Analysis
- Dynamic Stress Analysis
  - Random Vibration Experiment
  - Random Vibration Stress Analysis - Numerical model

The work structure presented is commonly used to study the dynamic behaviour of a structure. Windscreens from the big car and the small car are selected and studied using the presented methodology.
The Modal Analysis phase will include windscreens from both car models while the Dynamic Stress Analysis phase will be limited to the study of stress distribution on the big car's windscreen. Figure 3.1, gives an overview of the flow carried during the course of this study.

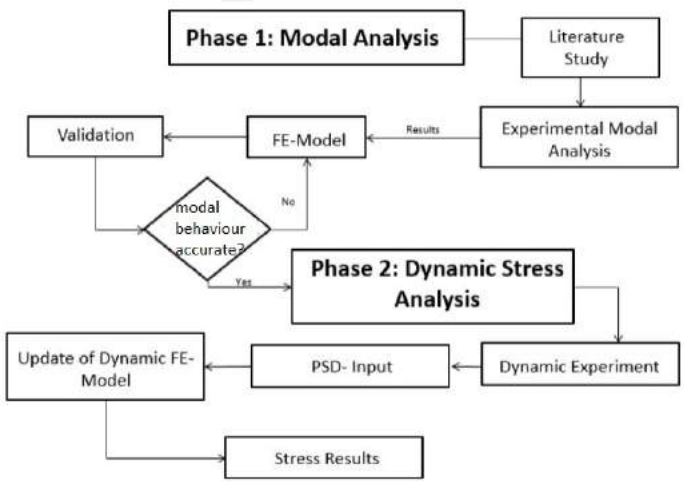

Figure 3.1: Project Method and Work Flow

3.1 Construction and Development of Finite Element Models

The first steps taken in this project was the construction of the finite element model of the two windscreen model. The CAD models of two windscreens was provided by VCC were imported into the pre-processing software ANSA [35]. Even through the laminate materials and its thickness remained same for both the windscreens, the big car variant was comparatively larger in size and dimension to the small car variant and had a larger curvature to it. Additionally, the mounting brackets which supports the rear view mirror and houses different sensors were different across the variants [3]. Keeping the distinctions in mind, one finite element model was constructed for each windscreen variant. During this phase the FE models were constructed using both 2D Shell and 3D Hexa elements. The iteration with the 2D Shell elements is carried out as they require less computational time to simulate a solid model in 2D space. 3D Solid elements are taken to be most accurate representation of any 3D body and the mesh produced provides a through the thickness variation of stress and strain and are used to validate the 2D Shell results. The different iterations of the finite element model constructed are shown in Table 3.1.

Test	Windscreen thickness (mm)	Type of FE Element	Material of laminate
1	4.46	PSHELL	All Glass
2	3.7	PSHELL	All Glass
3	4.46	PSOLID	Glass-PVB-Glass
4	4.46	PSOLID	All Glass
5	4.46	PCOMP	Glass-PVB-Glass
6	4.46	Extruded PCOMP	Glass-PVB-Glass

Table 3.1: Different iterations of the FE model construction

In iteration 1, the windscreen was meshed with a 2D Quad shell element with the element size of 5mm. The surface was then assigned with a thickness of 4.46mm which corresponds to the overall thickness of the windscreen. In the 2 iteration, thickness corresponding to PVB was removed from the thickness assigned to the PSHELL element with all the other parameters kept similar to the previous trial. This iterations helped in the study of the effect of thickness on the modal behaviour of the windscreen.
In iterations 3 and 4, the FE structure was constructed using 3D solid Hexa elements with element size of 5mm, with the introduction of the PVB layer. These iterations helped in understanding the effect of the plastic interlayer on the modal behavior of the windscreen.
In iterations 5 and 6 the laminate structure was kept similar to the previous trial, but the FE type was changed from PSOLID to PCOMP to study the variation of results due to the change in construction of the finite element.
During the course of all the iterations, the Young's modulus and the Possion's ratio of glass and PVB were used as in Table 2.1 and Table 2.2. As per the initial assumption, the materials were considered to exhibit linear elastic and isotropic behaviour. Figure 3.2, shows the constructed numerical model.

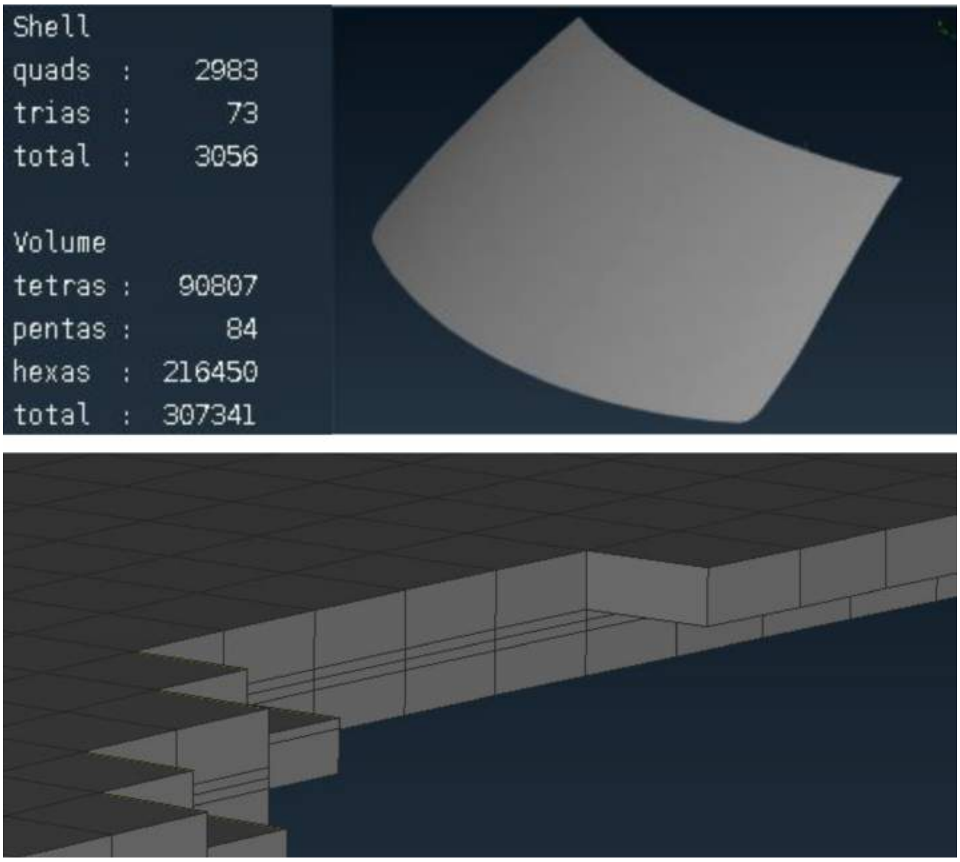

Figure 3.2: Numerical model of the Windscreen

After the construction of the numerical model in the pre-processing software ANSA, commercial FE solvers are used to solve the mathematical equations associated with the requested output. During the course of this study, the numerical models were solved using the FE code MSC Nastran, which is developed by MSC Software [37]. In this modal analysis is carried out using the solver SOL101 [37], which gives the output of the natural frequencies and the modes associated with it which is visualized in the post processing tool META [36].

As stated earlier, the PVB layer with its thickness of 0.76 mm represents a volume close to 23 % of the total geometry. This coupled with large change in the strength and mechanical properties of glass and PVB makes it vital to understand the influence of PVB on the overall dynamic behavior of the structure. Therefore, the various iterations of the numerical model help in understanding the interaction of the different layers of the laminate and its overall effect on the dynamic behavior of the windscreen.

3.2 Modal Analysis

In order to study the random response of the windscreen, it becomes vital to know the modal response of the system, which will help to understand which frequencies have the largest impact on the structure [23]. It is a general principle to include as many modes as possible to get the most accurate result.
However, including many modes increases the computation time and the process becomes cumbersome. So sufficient number modes are chosen with the highest mass participation factor. A mode with high mass participation factors is usually a significant contributor to the structural response of the system. Modes are selected such that it at least has a contribution of 2% of the total mass of the system [26][23].
The study of natural frequencies of the system helps to identify the material parameters of the laminate structure [24] and also forms the initial step in the random response analysis. So the parameters of the modal analysis setup are selected such that modes associated with the frequency range of 1-100Hz are simulated. This range of frequency is of interest, because it matches the PSD profile used to simulate transport conditions [21] [19].
From previous studies conducted on the study of modal properties of thicker windscreens [24], the first modes and its associated natural frequencies ranging from 1-50 Hz are usually associated with having higher stain energy and thereby cause greater displacement during vibration. It is also true of the windscreen structure to possess high damping factors at higher range of frequencies which makes it difficult to obtain clear cut peaks in the FRFs being calculated during the experimental modal analysis setup.

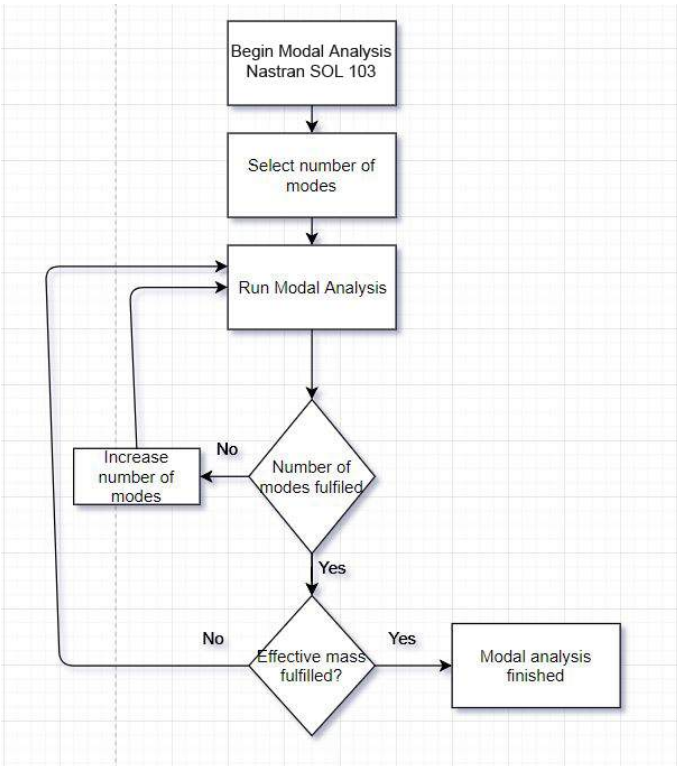

Figure 3.3: Numerical Modal analysis work Flow

Figure 3.3, shows the steps followed in calculating the modal characteristics of a structure. As the FE-model is not subjected to any boundary conditions, the natural frequencies and its corresponding mode shapes are only influenced by the material properties of the laminate. Initially the material parameters suggested by [27] shown in table 2.1 and 2.2 were used to simulate the modal response of the windscreen.
The resulting natural frequencies and the corresponding mode shapes helped identify the areas of interest where accelerometers can be placed during the experimental setup to capture all the modes of interest. This was done in order to validate the behavior of the numerical model against experimental data which later on lead to optimizing the material properties of the laminate through trial and error in order to obtain a close match between the numerical and the experimental results.

3.2.1 Modal Analysis - Experimental Setup

The EMA carried out on the windscreen specimen forms the physical testing part of the validating the numerical model. It is recommended as part of any methodology involving numerical modelling that validation of numerical results against experimental results always help optimize the numerical model to predict the most accurate structural behavior.
So in order to validate the constructed numerical model 3.1, a physical modal analysis experiment is setup in the NVH laboratory at VCC. The test setup is as shown in figure 3.4. The windscreen is hung to a support structure using soft bungees, which simulates the free-free condition i.e. there is no effect of any boundary conditions

or external forces acting on the body. Accelerometers were calibrated and placed at areas of interest predicted by the numerical model. Hammer impacts were used to excite the structure and the reading from the accelerometers were captured using the tool LMS TestLab, which is developed by Siemens PLM software.

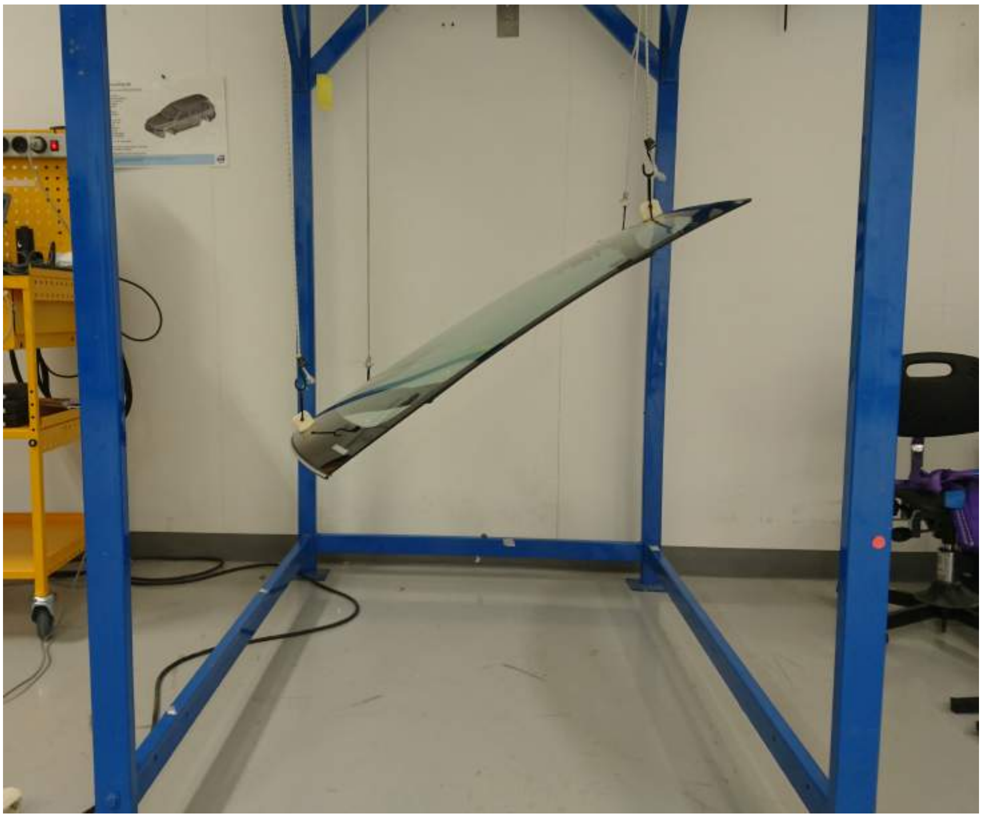

Figure 3.4: Experimental Modal analysis -Test Setup

The principle behind the selection of excitation points and accelerometer placement points is that exciting a structure at different points leads to multiple FRFs being calculated. These FRFs will have different shapes with frequency peaks being registered at one data collection point i.e. at one of the accelerometers, and the other peaks being registered at other sensor locations. So it becomes vital to have the placement of sensors in such way that it leads to most of the frequency peaks being captured. Care is also taken such that no excitation or response points lie on the nodal line of any modes as the input energy might not be well transferred to excite the mode [26]. Keeping this in mind, the excitation and the sensor locations on the windscreen are selected and shown in figure 3.5. Where, points 1-7 show the response points and 34 impact points on the windscreen.

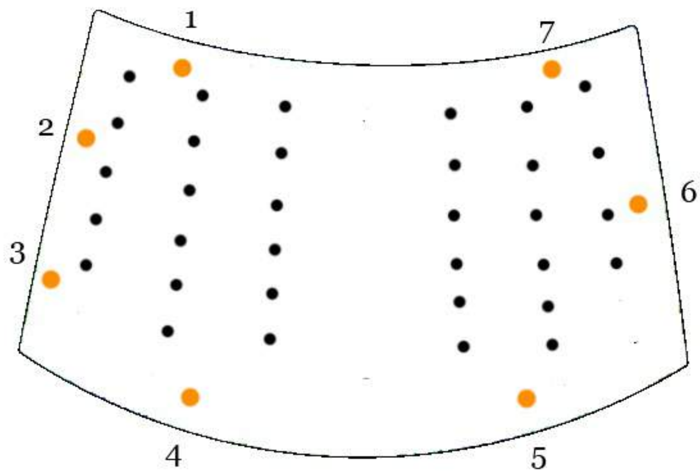

Figure 3.5: Overview of the measurement points (black) and accelerometers (orange)

As the experiment was carried out, the impact hammer was first calibrated so as to avoid any erroneous impacts being recorded and the windscreen was excited 5 times at each excitation point and the coherence function was recorded and checked if any abnormalities in the readings were detected, the trial was carried out again until the coherence function was varying between acceptable limits.

As discussed earlier, the choice of the impact hammer along with its tip material plays a vital role in achieving a good result. With glass being a brittle material and the laminate having good damping properties, the rubber tip was selected for the hammer. As a rubber tip was used, the cutoff frequency was quite low ranging at 180-200Hz which still was above the requested range of study at 100Hz. Figure 3.6 shows the impact hammer used with its rubber tip.

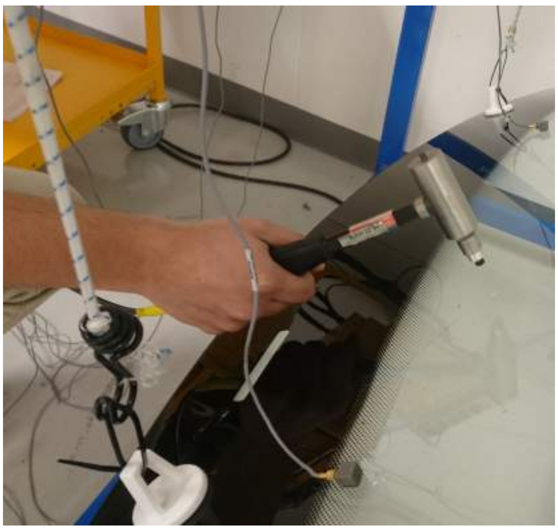

Figure 3.6: Impact hammer excitation

During the experiment, accelerometers were used to measure the acceleration of the excited structure. Seven accelerometers were glued to the surface of the windscreen using hot wax and placed at points 1-7 as shown in figure 3.5 and were placed on the top surface such that the acceleration direction was out of plane of the windscreen as shown is figure 3.7.

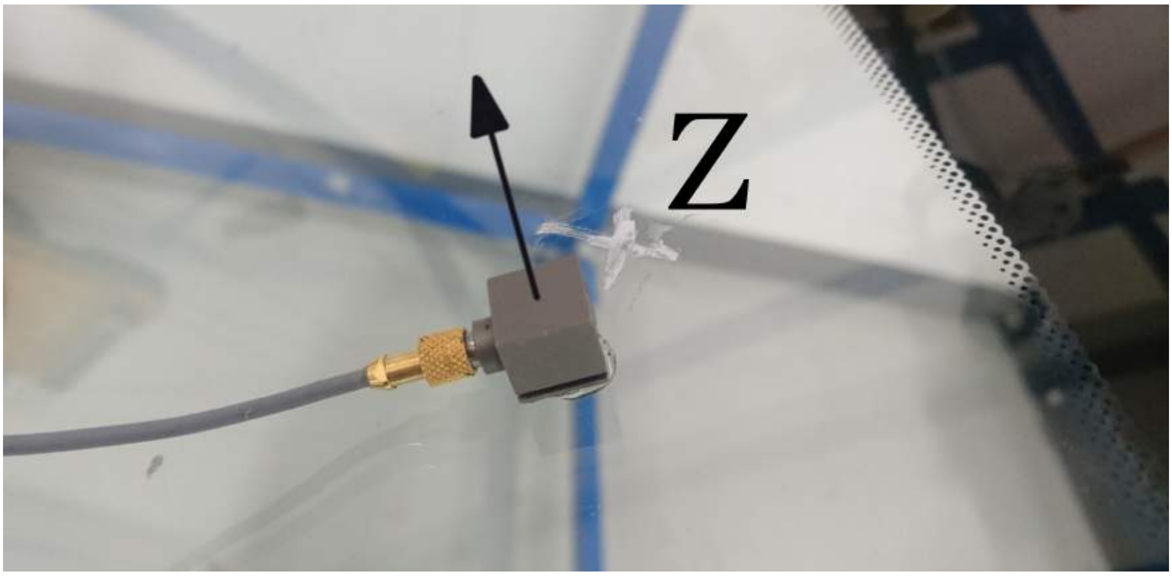

Figure 3.7: Accelerometer placement and orientation

As the accelerometers were glued to the surface of the windscreen, the hammer was used to excite the windscreen structure and the FRFs generated were captured using the software LMS TestLab. After capturing the acceleration data a wireframe model of the windscreen is constructed, figure 3.8 in LMS TestLab and the recorded FRFs are used to simulate the dynamic behaviour of the wireframe model.

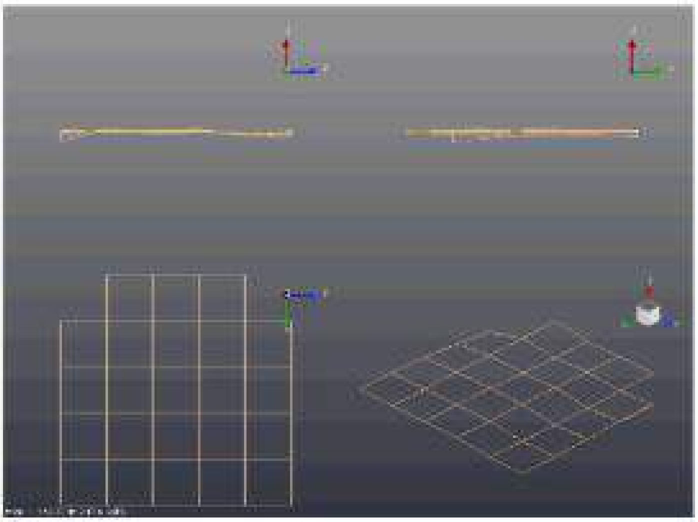

Figure 3.8: Constructed wireframe model of windscreen in LMS

With the described sampling technique, and analysing the captured data made it possible to visualize the experimental mode shapes and provided insight into the natural frequencies of the structure.

3.2.2 Validation of FE models - Modal Analysis

After the experiment was carried out, the output data from the experiment such as FRFs, mode shapes and natural frequencies of the system were analyzed and tabulated. These results were then used to validate the modal behaviour predicted by the numerical model.
As written earlier, because the structure was analysed in the free-free condition, was the dynamic behaviour predicted by the numerical model solely dependent on the mechanical material properties of the constituents of the glass laminate structure. This along with the assumption of linear isotropic behaviour made for both glass and PVB only leaves out Young's modulus 'E' and Possion's ratio 'ν' as the variable parameters that can influence the dynamic behavior of the windscreen.
This coupled with the fact that both glass and PVB have a range of values for Young's modulus and Possion's ratio 2.1, 2.2, makes this a good parameter study on the effects of Young's modulus and Possion's ratio on the dynamic behavior of the structure.
So a trial an error approach is adopted where the frequency response from the experiment is used as the base and the material properties of glass and PVB are varied to until the most accurate resemblance to reality is achieved. This is done by updating the material card in the pre-processor and the results obtained from each iteration are visually compared with the experimental results.
The material parameter set which yielded the best match to the experimental results are presented. Due to the nature of visual validation, it becomes difficult to accurately compare the mode shapes at frequency ranges above 100 Hz as the shapes become more complex with the increase in frequency.

3.3 Random Vibration Analysis

After the validation process carried out, the numerical model of the windscreen with its optimized material card is simulated for random vibration analysis.
The methodology used in determining the random response characteristics of the system consists of the following steps. First are the normal modes of the system calculated, the steps are followed in numerical modal analysis, followed by obtaining the normal modes of the system. This is followed by applying the PSD load case to the system and the random response is simulated. Then the RMS value of the response PSD is calculated and presented [23]. Figure 3.9 shows the work flow of random vibration.

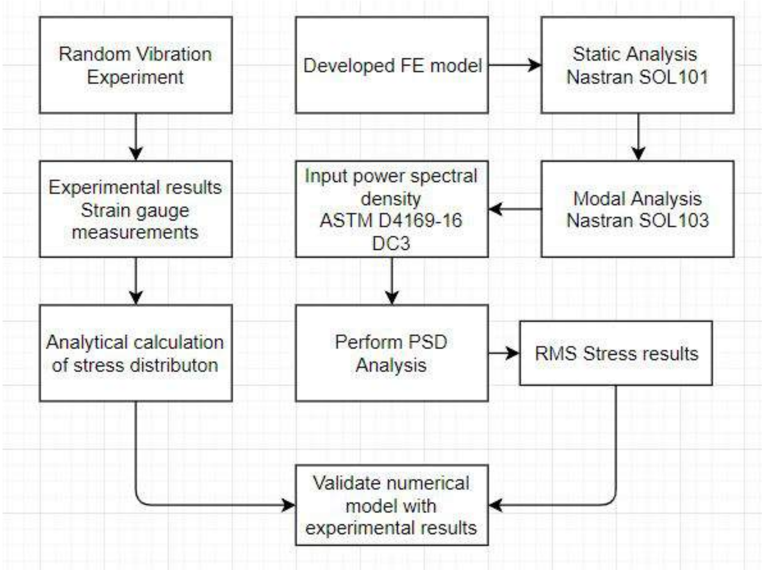

Figure 3.9: Flowchart for pre-stressed random vibration simulation

3.3.1 Update of FE-Model

When the numerical model was constructed in earlier, see section 3.1 there were no boundary conditions acting on the structure. This was done in order to simulate the structure in a free-free environment. However, with the case of random vibration which is used to simulate the transport vibrations it becomes essential to have the boundary conditions which simulate the actual packaging method.
To that effect the numerical model is revisited and updated with the boundary loads and constraints that the windscreen structure will experience during transportation. Figure 3.10, shows how the windscreens are stacked in racks before and during transportation. As seen in figure 3.10, the windscreens are held at six locations with the help of plastic spacers and straps.

Figure 3.10: Packaging of windscreens for transportation

The boundary setup seen in figure 3.10, was translated into the numerical environment and the constraints and loads. The FE-model were updated according to observation with fitting boundary conditions, constraints and forces, seen in figure 3.11, to replicate the ideal boundary conditions and strapping forces acting on the windscreen stack during transportation.

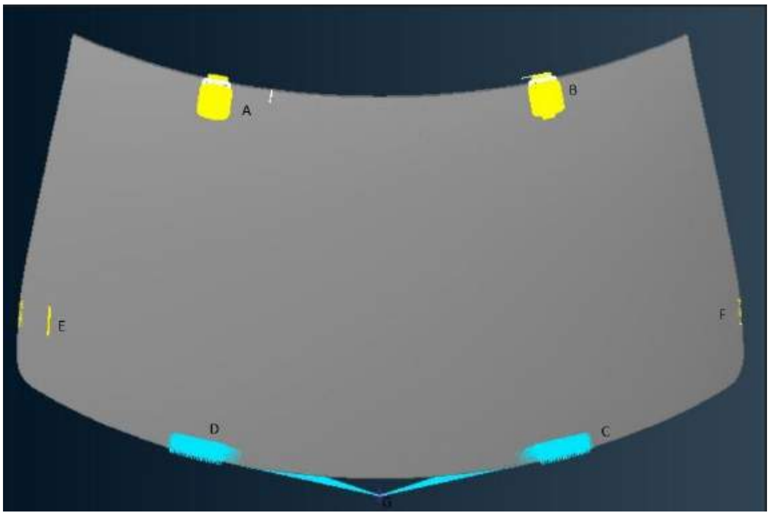

Figure 3.11: The constructed FE model imitates the transportation rack

The constraints present on the top spacers denoted by letters ’A’ and ’B’ in figure 3.11 simulate the strapping force exerted by the plastic straps which are tightened with a force of 400 N [2]. The straps run through the top surface of the spacer and are held down as shown in figure 3.12.

Figure 3.12: Strapping of windscreens

Figure 3.13: Tilting windscreens representing the rear force

It is also evident from the figure 3.12, that the windscreens are stacked in such a way that consecutive spacers are always in contact and so certain amount of the weight of one windscreen falls on the one behind it and so the last windscreen held by the orange spacer experiences the weight of all the windscreens falling on it. The stacking of windscreens results in a rear force of a 13 N force per windscreen which amounts to a total force of around 180 N and is modelled as a compressive force acting on the last spacer. Lastly it can also be seen that the last spacer (orange), rests on the support of the rack, in order to mimic this, the nodes are constrained in the X and Y directions. An enhanced image of the spacer with the applied loads and constraints is shown in figure 3.14. The contacts between the spacer and the windscreens were modelled using rigid body RBE3 elements.

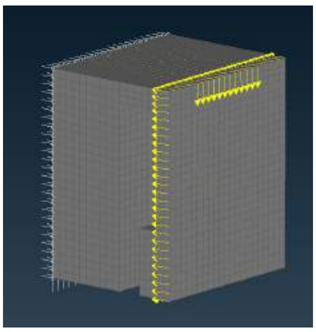

Figure 3.14: The contacts between the brackets and the windscreen

The constraints to the sides of the windscreen marked by areas 'E' and 'F' in figure 3.11, are also modelled as compressive loads with a force of 400N [2] acting along the surface of the windscreen in the Z direction. The application of loads is illustrated in the figure 3.15.

Figure 3.15: The side boundary force holding in Z-direction

The bottom supports of the rack have similar function as the top spacers and they prevent any movement of the windscreen in the X and Y directions. As this boundary should support the input PSD load, which in general practice is applied to a single node in Nastran [37], all the nodes in contact with the supports are connected to a single master node using rigid body elements (RBE2). Then a single point constraint or SPC is applied on this master node such that it simulates all the connected nodes being constrained in the X and Y direction. Then the random vibration load PSD is applied along X axis (Vertical direction) to the same master node to simulate forced random vibration. The boundary setup in the numerical model is depicted by figure 3.16.

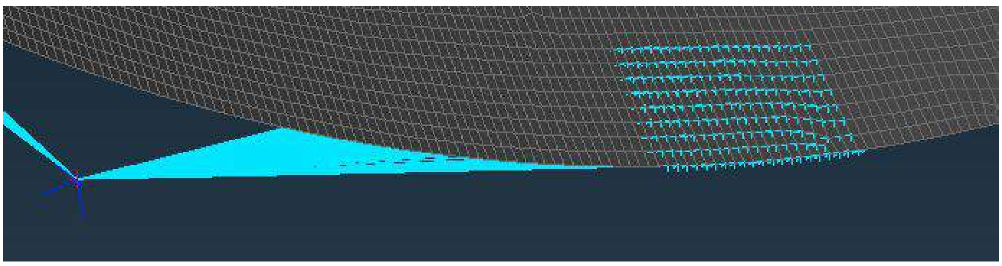

Figure 3.16: The boundary supports connected with RBE2 contacts to the SPC1 constrain

When the windscreens were modeled during the modal analysis phase of the project, some of the plastic brackets which are used to house the rain sensors and the rear view mirror were not modeled. However, now during the dynamic stress analysis it becomes vital to understand how these brackets which are glued on to the rear surface of the windscreen affect the stress distribution. Figure 3.17 shows how these brackets are positioned on the windscreen and figure 3.18, shows the numerical representation of the brackets in the preprocessor.

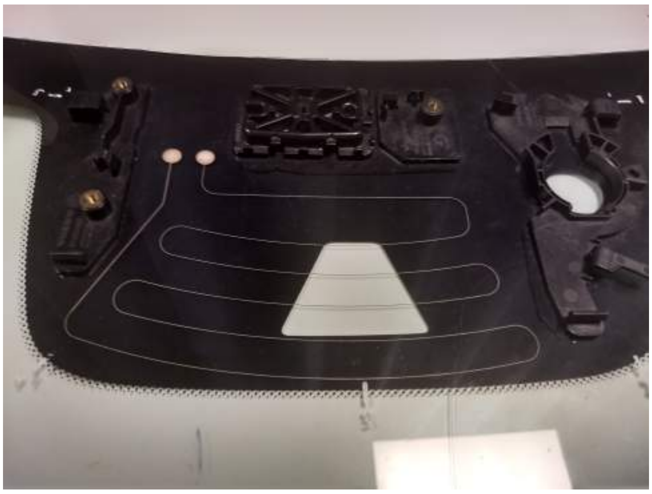

Figure 3.17: Plastic brackets glued on rear surface of windscreen

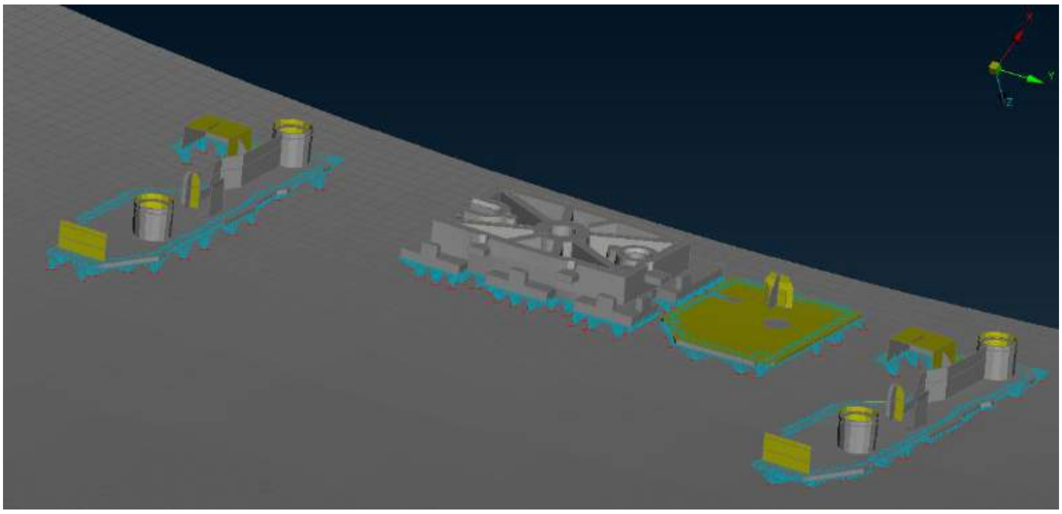

Figure 3.18: Numerical modeling of the plastic brackets

In total, four such brackets were modeled. The positioning of the brackets is unique to the big car model. In reality, these brackets are glued on to the surface of the windscreen which creates an adhesive contact between the two surfaces. In the numerical model however, the contacts are modeled using RBE3 element which is a rigid body interpolation element. The RBE3 element is constructed in such a way that nodes on the brackets form the master nodes and the nodes on the windscreen form the slave nodes.

Out of the four brackets modeled, three of the brackets are constructed using shell elements while the rear view mirror holder was constructed using solid element due to its complexity. Each shell structure is meshed with quadratic elements and the solid structure is meshed with penta-elements. A mesh size of 2 mm is kept constant during the construction of all the brackets.

With all the applied boundary conditions and loading, a complete functional model with components and operating boundaries integrated in the structure as the transportation rack is constructed and presented.

3.3.2 Stress Analysis

The vibration experiment is performed on one of Volvo's transportation rack with a total of 15 windscreens. These windscreens are unique to the big car model. From previous transportation studies [21], [20] this test is carried out to simulate the vibrations induced during transportation and its impact on the windscreens being transported. As stated earlier, parameters such as the driving speed and road conditions control the transportation quality. For instance, driving on unevenness roads (laterite roads) and potholes has increased levels of vibration than driving on a stable road condition (concrete or asphalt). These high vibration levels could potentially produce vibration damage to the products. Due to the limitation unable to conduct the testing on an actual truck in service, a truck simulation standard load is used to excite the rack. The experiment is carried according to the ASTM standard, ASTM D4169-16 DC3 [19] standardized truck vibration with three level profiles. The profiles are labeled as high, medium and low levels and uses a spectrum, Figure 3.19, shows the input spectrum used to excite the test rig, a servo-hydraulic vibrator, is used to convert the input electronic signal into mechanical movement of the test rig which in turn induces the random vibration onto the windscreen rack both in lateral and vertical direction. But due to the rack being heavy, the frequency input to the test rig is limited to 30Hz. The PSD input used for the experiment was collected and was given as input to the numerical model and the RMS stress results obtained were analyzed.

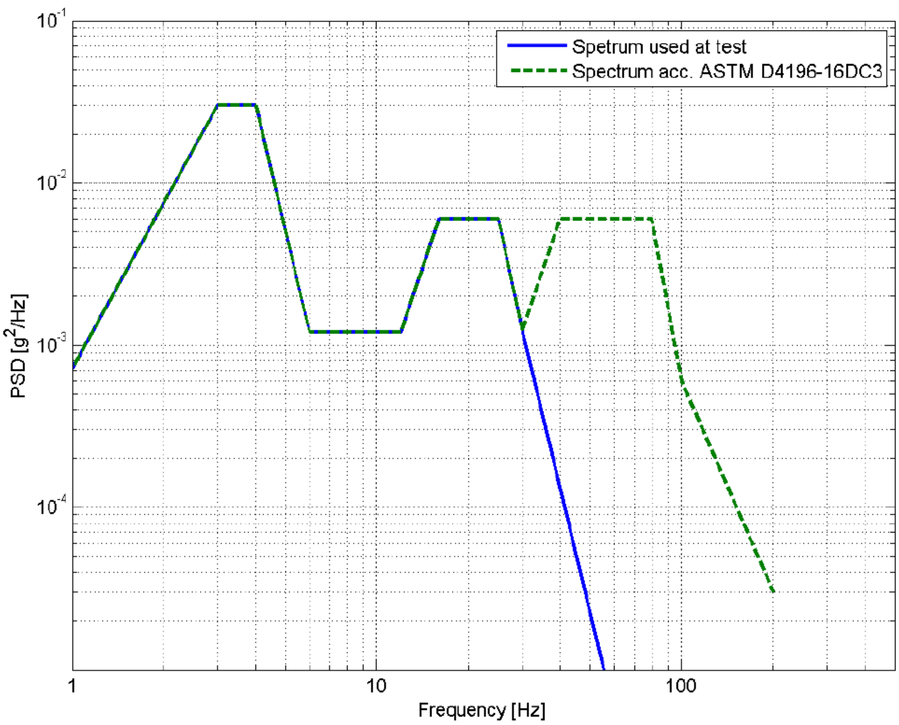

Figure 3.19: The inserted spectrum to the test rig [38]

The experiment is carried at Research Institutes of Sweden AB (RISE) [22] located at Borås, Sweden. The windscreens are stacked in accordance to the packaging instructions by VCC, and are held in position by forced straps [2]. The experiment is carried along by placing 10 strain gauges at various user defined critical areas showcased in figure 3.20. These strain gauges measure the local strains in all the three directions. The strain gauges are of type SKF 24769 from KYOWA. An enhanced view of the mounted strain gauge is shown in figure 3.21.

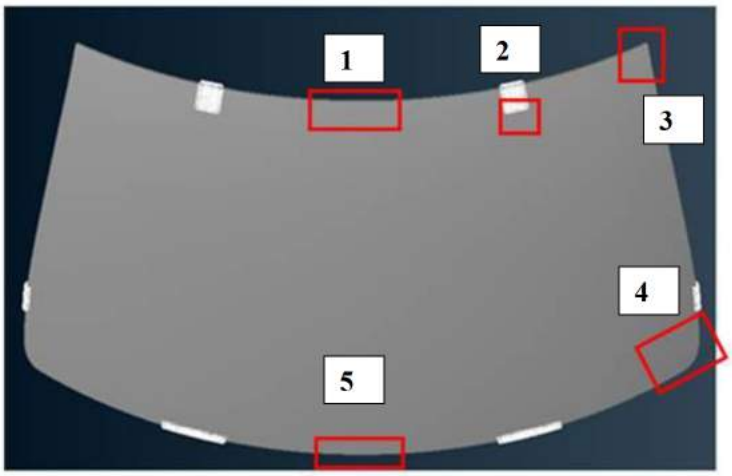

Figure 3.20: The positioning of the gauges on the windscreen

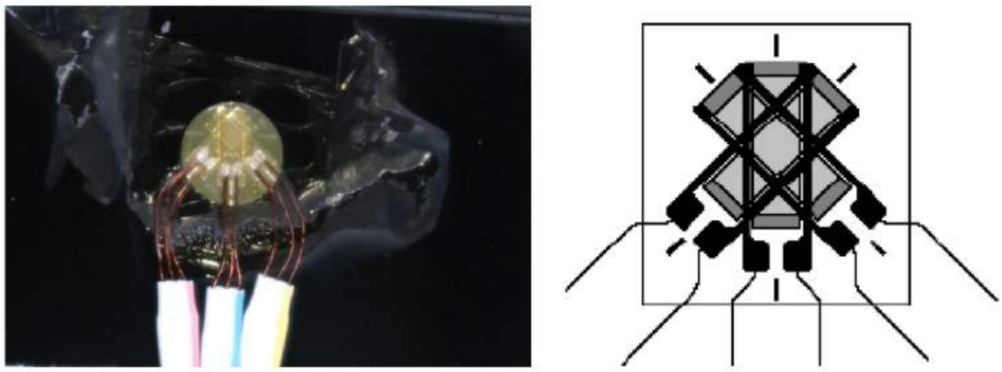

Figure 3.21: A close-up on the gauge and its wire at a 45 degree angle [38]

The first run is carried out with strain gauges mounted on the first and the last windscreen in the rack. The obtain strain measurements gives an idea of the variation of strain between the first and the last windscreen. The second experimental run is carried out with the strain gauges mounted on the windscreen positioned in the center of the rack. The first windscreen is scratched along its edges. The scratches are made at 50 mm from the edge using a 80-grit sandpaper with a weight of 1.5 kg used to pressure the sandpaper against the glass. These scratches are induced to study the effect of any small imperfections causing higher stresses in the windscreen. The scratch test carried out however has no literature backing or a standardized testing procedure.
The local strain measurements are then used to calculate the stress distribution at those areas and are used to validate the stress results calculated using the numerical model. The analytical calculations are carried out according to equation 4.1.

4

Findings and Analysis

In the following chapter, the results obtained by applying the stated methodology are presented. The presented results follow the same work flow as described in methodology, see section 3. Initially the results obtained from the numerical modal analysis are presented for the two windscreens followed by the experimental modal analysis results, later on, the validation results between the numerical and the experimental results are presented. The modal analysis results are followed by the results pertaining to the random frequency response experimentation and numerical analysis along with the validation of the numerical results is presented.

4.1 Phase 1: Modal Analysis Results

In this section, the results from the numerical and experimental modal analysis are presented which is followed by the validation of numerical results with experimental data.

4.1.1 Experimental Modal Analysis

As the windscreen was excited using hammer impacts, the recorded data was sampled up till 100 Hz, and the FRF peaks captured are shown in figure 4.1.

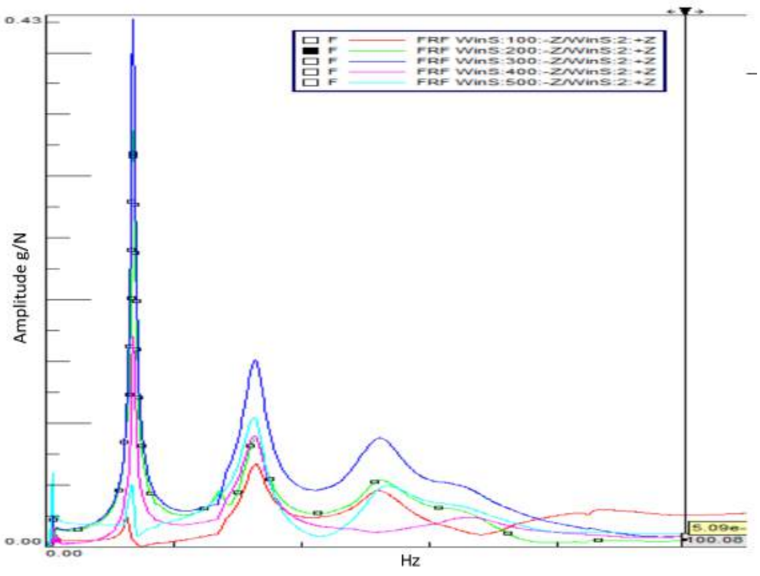

Figure 4.1: Plot of FRF captured sampled at 100 Hz

The peaks seen in figure 4.1, are representative of the natural frequencies of the system and the various colours in the plot represent the data from different sensors. The natural frequencies recorded by the 7 accelerometers and the modes associated with these frequencies for the two windscreen models are tabulated and shown below:

Windscreen 40	Experimental Modal Analysis						
Ref/Acc	1	2	3	4	5	6	7
1	12.662	12.654	14.022	12.668	12.689	14.046	12.604
2	33.770	14.044	33.806	14.024	30.897	30.887	30.799
3	54.001	30.763	53.981	30.905	33.756	33.720	33.715
4	56.889	33.656	57.408	33.673	57.683	54.025	54.165
5	72.400	53.818	78.848	54.088	97.930	57.772	72.298
6	79.275	57.415	113.630	79.138	151.164	72.434	85.988
7	104.131	72.485	140.063	97.699		79.121	113.265
8	113.567	78.218	167.272			171.704	139.410
9	118.748	98.314				194.133	
10	140.002	113.652					
11	154.338	134.571					
12		152.252					
13							

Figure 4.2: Experimental results windscreen - Windscreen B

Windscreen 90	Experimental Modal Analysis						
Ref/Acc	1	2	3	4	5	6	7
1	12,727	13,345	13,454	12,618	12,646	13,462	12,56
2	27,658	27,69	27,692	13,351	32,442	27,664	27,714
3	32,462	32,439	32,458	27,738	49,555	32,45	32,447
4	49,423	49,838	48,718	32,474	71,269	51,793	49,518
5	50,874	92,147	51,546	49,262	86,049	65,848	70,87
6	52,424		92,85	65,813	117,156	115,831	86,592
7	70,82		116,858	137,59	178,845	145,707	135,952
8	86,291		180,04	181,84		177,138	180,621
9	119,476					180,177	
10							
11							

Figure 4.3: Experimental results windscreen - Windscreen A

In both tables, the first column shows the mode numbers and the first row shows the sensor number ranging from 1-7 which were placed according to figure 3.5.
The positioning of the accelerometers is seen to have a significant impact of the documentation of the response mode shapes. Depending of the placement different sensors did detect various mode shapes. The small car's windscreen is seen to be able to sample more mode shapes than the big car's windscreen.

4.1.2 Finite Element Analysis

As stated in the methodology, see section 3, different iterations of the numerical model were constructed in order to get a comprehensive understanding of the effect of various parameters may have on the simulated result. The results from the different iterations are tabulated.
Excluding the PVB interlayer led to a decrease in the natural frequency of the system. As the PVB layer in the windscreen structure has a thickness of 0.76mm which is a significant portion of the overall thickness amounting to 18% of the overall thickness, the omission of the layer leads to a structure with higher stiffness. This

coupled with the lack of damping leads to frequency peaks at lower values. The results from the parameter study on the influence of different element structures for the two windscreen structures are shown in figure 4.4 and figure 4.5. In reality the laminate structure of the windscreen experiences shear in the interlayer, which is accurately depicted when using solid hexa elements. This shearing is not taken into account when the structure is modeled using shell elements, hence the modal results from the solid element iteration is taken in as the base for further validation with the experimental results.

Mode	Shell 3.7 (Hz)	Shell 4.46	Shell Composite	Solid_Glass (Hz)	Solid_GPG (Hz)	Solid Laminate (Hz)
1	11,85	14,28	14.62	14.27	14.69	14.64
2	12,43	14,85	15.35	14.85	15.38	15.35
3	28,96	34,63	35.53	34.59	35.43	35.34
4	31,75	37,89	38.87	37.87	38.96	38.89
5	51,43	61,24	62.14	61.17	62.35	62.22
6	54,55	64,83	65.84	64.76	66.04	65.92
7	71,97	85,54	86.29	85.42	86.54	86.43
8	78,64	92,8	92.90	92.65	93.27	93.07
9	100,37	1196,38	120.55	119.25	120.76	120.69
10	113,87	134,1	134.11	133.91	134.55	134.32
11	137,6	162,65	162.53	162.44	162.92	162.78
12	139,97	163,9	162.96	184.57	163.45	163.23
13	158,4	184,84	183.46	214.19	183.82	183.76
14	183,78	214,49	211.90		212.43	212.25
15	195,67					

Figure 4.4: Modal Results for windscreen B

Mode Shape	Shell 3.7 (Hz)	Shell 4.46 (Hz)	Shell Composite (Hz)	Solid_Glass (Hz)	Solid_GPG (Hz)	Solid Laminate (Hz)
1	11,09	13.35	13,74	13.40	13.81	13.81
2	14,41	13.66	14,17	13.69	14.19	14.19
3	26,4	31.6	32,35	31.71	32.49	32.49
4	29,98	35.76	36,81	35.82	36.88	36.89
5	50,14	59.66	60,82	59.82	61.03	61.04
6	51,71	61.38	62,68	61.49	62.84	62.85
7	71,75	84.37	84,95	84.57	85.25	85.27
8	73,99	87.62	88,72	87.79	88.98	88.99
9	98,81	117,03	118,19	117.16	118.54	118.57
10	100,92	117,97	118,38	118.19	118.60	118.63
11	129,77	152,95	153,66	153.11	153.99	154.02
12	137,04	159,74	159,73	159.96	160.10	160.13
13	159,82	185,59	184,76	185.70	185.06	185.09
14	162,6	187,95	186,56	188.09	186.94	186.98
15	188,48	206,93				
16	196,09					
17	201.25					

Figure 4.5: Modal Results for windscreen A

4.1.3 Modal Analysis Validation

After the application of the validation methodology described in section 3. The material cards in the numerical model were optimized in order to get a good behavioural match between the numerical and the experimental data. The change material properties in the FE-models displayed no distinguishable change of mode shapes, except from a change in the frequency range. The procedure of changing the stiffness of the material was carried out by varying the Young's modulus in the material card. The most accurate match between the numerical and the experimental data was achieved with the material parameters shown below.

	Young's Modulus (GPa)	Density (g/mm^3)	Poisson's Ratio
Glass:	72	2.2	0.23
PVB:	0.343	1.1	0.49

Figure 4.6: The selected material card

Figure 4.7, shows the first six critical modes of the structure, these modes are associated with frequency values that are presented in figure 4.5.

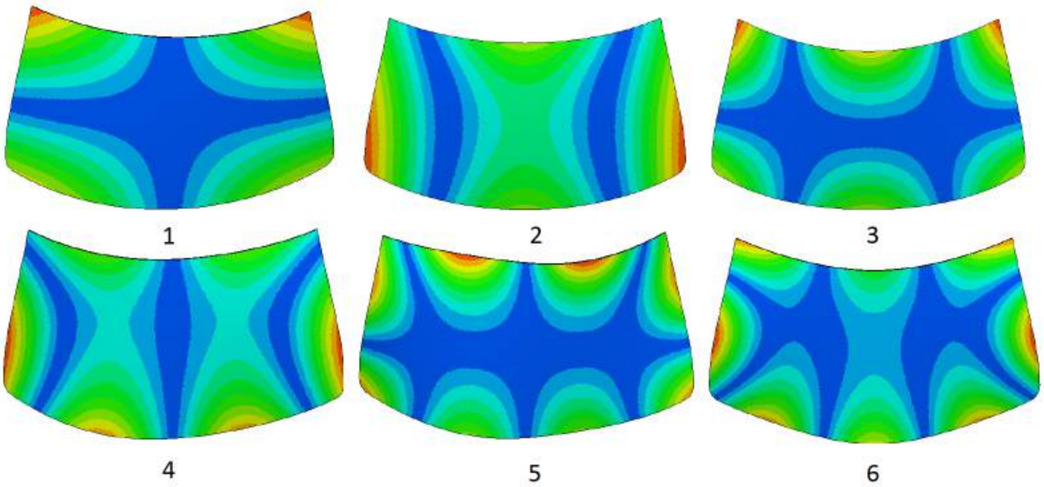

Figure 4.7: Windscreen A's first 6 mode shapes

The colours of the figures represent the body displacements of the structure, ranging from the colours blue to red. The blue colour demonstrates low displacement, while the red colour demonstrate the maximum displacement of the structure for a particular exciting frequency . Figure 4.7 illustrates that low activity is occurring at the middle part of the structure, while the edges and corners are exposed to larger displacement. As the structure is simulated in the free-free environment, the first 2 modes show the body showing a flexural wave form. The mode shapes shown by the structure at elevated frequencies become more complex as is evident from figure 4.7 and the frequencies associated with the mode shape are shown in figure 4.8. The results from the experimental modal analysis shown in figure 4.8 are used to validate and calibrate the material card in the FE analysis. As it is evident from table 2.1

and table 2.2 the Young's modulus and poisson's ratio for glass and PVB have a range of values and as the modal response of the system is influenced by the stiffness of the system which in turn is influenced by the Young's modulus and the Poisson's ratio the material card in FE analysis was calibrated by validating the modal response results with the experimental data. A method of iterative calibration was adopted and the material card thus developed was also validated against literature sources [4]. The material card developed was consistent with the results from the literature as the frequency response predicted by the numerical model was in close relation with the experimental data. As normal mode extraction is the first step towards predicting random response [23] having a optimized material card become vital the results of which is put forth in this chapter.

Mode	Solid hexa GPG (Hz)
1	13.81
2	14.19
3	32.49
4	36.88
5	61.03
6	62.84

Acc 1 (Hz)	Acc 2 (Hz)	Acc 3 (Hz)	Acc 4 (Hz)	Acc 5 (Hz)	Acc 6 (Hz)	Acc 7 (Hz)
12,7267	-	-	12,618	12,6458	-	12,5602
-	13,3446	13,454	13,351	-	13,4616	-
-	27,6899	-	27,738	-	27,6644	27,7145
-	32,4392	32,4577	32,4737	32,4419	32,4505	32,447
-	-	-		-	65,8484	-
-	-	-		-	-	70,8702

Acc: Accelerometer

Figure 4.8: Modal validation between EMA and FE- modal analysis for windscreen

4.2 Phase 2: Dynamic Stress Analysis Results

4.2.1 External vibration data

The physical random response experiment conducted at RISE, provided the input PSD load to be applied during the numerical modeling. As stated in the methodology see section 3, The input PSD had to be limited to 30 Hz due to the weight and volume of the rack. The PSD – signal sampling rate was 600 Hz, with Nyqvist Therom gave the sampling period of 300 Hz with highest activity below <50 Hz as seen in figure 4.9.

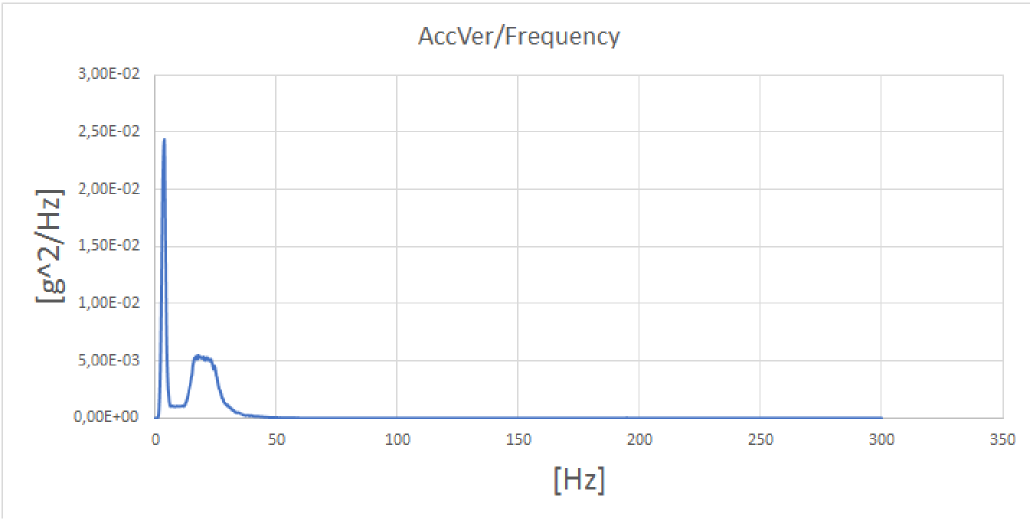

Figure 4.9: The sampled PSD- signal up to 300 Hz

The results from the strain gauges mounted in five areas on the windscreen were analysed and it was observed that the strain gauge closest to plastic spacers recorded higher strain rate over the period of application of load. The strain gauge at area 2, close to the upper right spacer, figure 3.20, had the highest strain and therefore best sampling result from the experiment. The summarized local strain result is presented in figure 4.10.

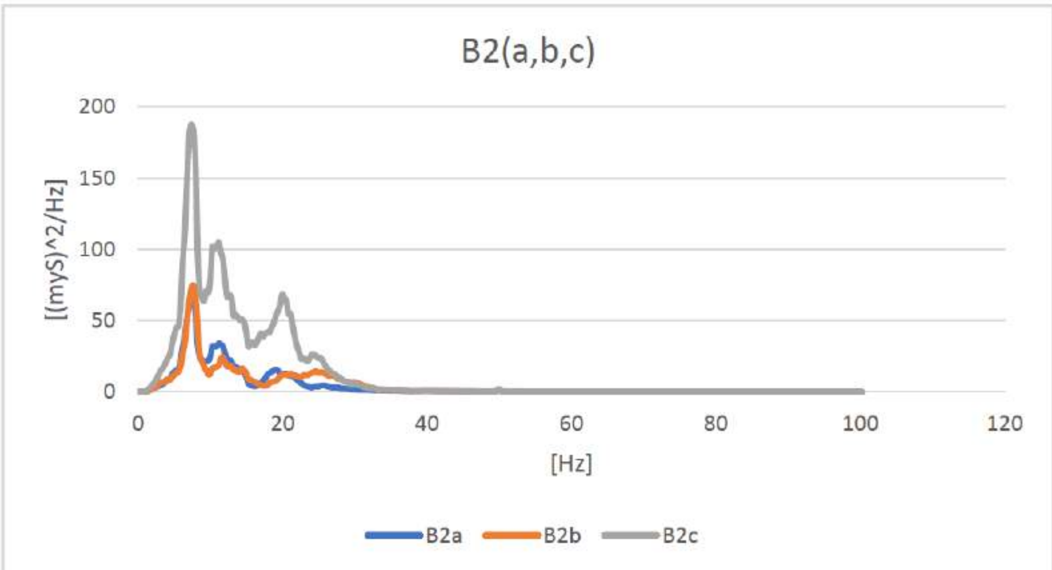

Figure 4.10: The strain results from the 2 gage ^{B}

From the strain rate seen in figure 4.10, the maximum principal stress is calculated using, equation 4.1. The gauge is placed one centimeter below the upper right spacer and resulted in a maximum stress of 14 MPa in the structure. The stress has no potential risk of breaking or damaging the glass layer at frequency range of 30 Hz.

$$\sigma_{max} = \frac{E}{2(1-v^2)}[(1+v)(\epsilon_a+\epsilon_b)+(1-v)\sqrt{2((\epsilon_a-\epsilon_b)^2+(\epsilon_b-\epsilon_c)^2)}] \quad (4.1)$$

The result from the two vibration tests demonstrated that the most vulnerable was the last windscreen in the rack (closest to the metal supports). The first simulation had no reports of visual damages to the tested windscreens. For the damaged windscreen of the second simulation resulted in crack formations. The first crack was observed in the transversal direction, the second crack after the longitudinal direction and the third crack in the vertical direction. It was perceived by inclusion in the laminate structure that close edges resulted in crack initiation and propagation, although the test was not critical due to the use of a non-standardized testing. The strain rates however were consistently higher near to the top right spacers for all the testing trials.

4.2.2 Simulation of the Dynamic Numerical Model

As stated earlier, the random vibration simulation starts of by identifying the normal modes of the constrained system. With the numerical model now being constrained to replicate the actual stacking orientation as seen in figure 3.11. The output mode shapes and their corresponding natural frequencies of the constrained structure are associated with 4.12. Repeating procedure of the modal analysis phase revealed a change in both mode shapes as in the frequency domain of the structure. The first subsequent mode is calculated at 9.568 Hz shown in figure 4.11 than 13.81 Hz in free-free condition figure 4.8. Here can is the deformation of the constrained FE-model be studied to investigate the displacement rate (measured in mm) represented by the colour scheme. Lower displacements are visualized as blue colour while the maximum are visualized with red colour. The mode shapes demonstrate behaviour of the structure at its natural frequency. The structure is having less deflection between the constrained boundaries. The highest displacement, the red colour, was once again found around edges and the corners. The highest displacement rates are appearing away from the boundaries due to the increased of stiffness. In these red areas, high displacement, can the windscreen oscillates and are of high interests from a resonance perspective.

Mode Shape	Frequency (Hz)
1	9.568
2	21.069
3	34.520
4	45.693
5	51.103
6	59.815

Figure 4.11: First six critical modal frequencies- constrained structure

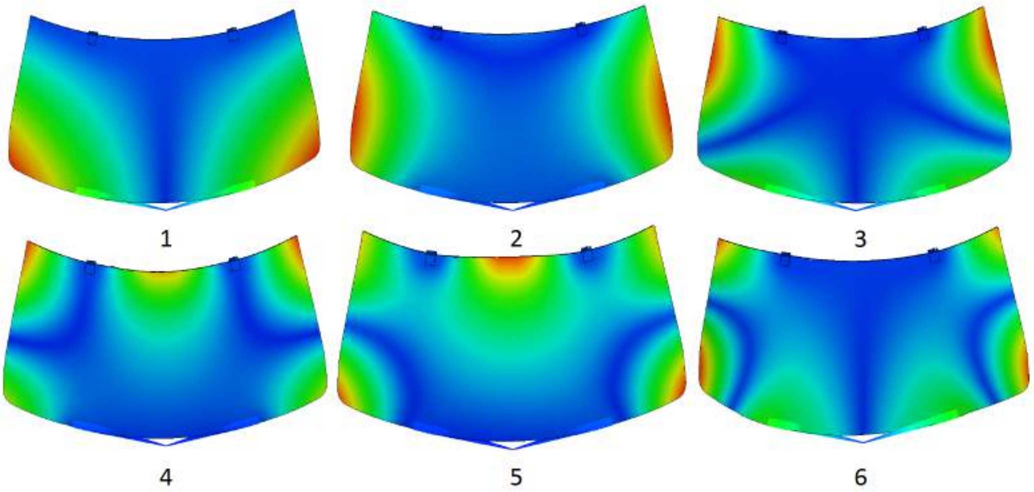

Figure 4.12: The windscreens' mode shapes when placed in the rack due to the boundary conditions

Inserting the PSD input to the SPC1 constrain, the windscreen was excited according to the profile. The figures 4.13 and 4.2.2, represent the stress behavior of the structured windscreen in static case before transportation (without PSD) and vibration state during transportation (with PSD) respectively. Both simulations revealed a higher stress activity close to the rack supports while the remaining structures are displaying a lower stress levels. Visualized from both the figures were the stresses greater for the top spacers than the remaining supports. The result was explained with the applied forces at the spacer, which contributed to a higher stress factor at these regions. In a vibration state induces higher stress regions which is significantly greater than for the static case.

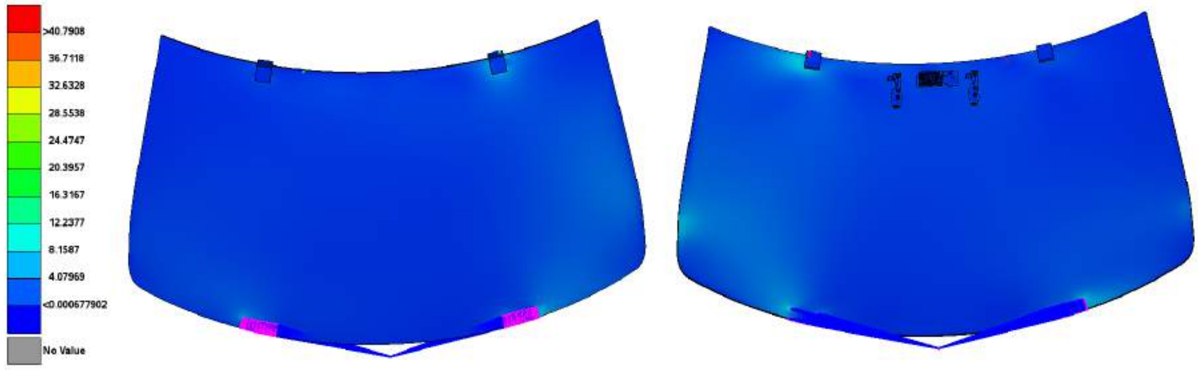

Figure 4.13: Von-mises principle stress- σ_1, Pre-stress state

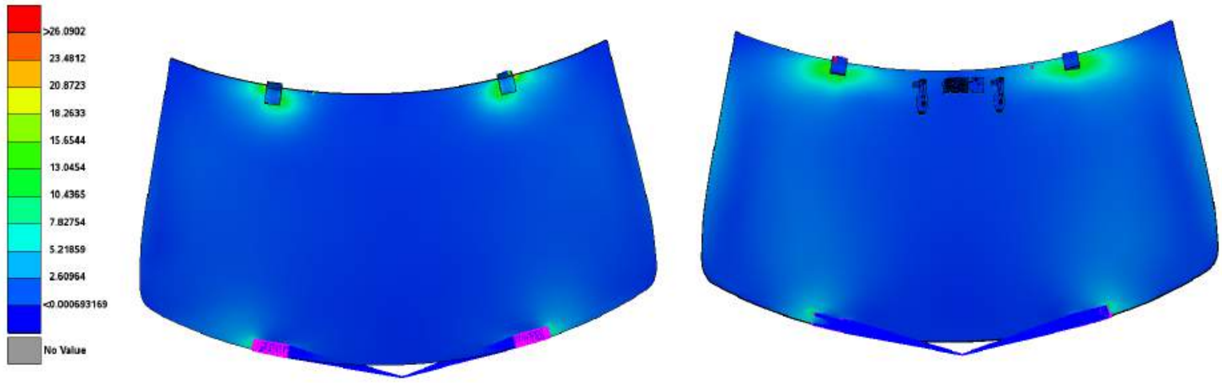

Figure 4.14: Von-mises principle stress- σ_1, Random vibration loads case

The validation will be made 1 cm below the upper right spacer, figure 4.15. For better demonstrations will a reference node be chosen for demonstration and ease for validation. Observing the plots of random vibration simulation show a high stress rate at the top of the top right spacer see figure 4.15

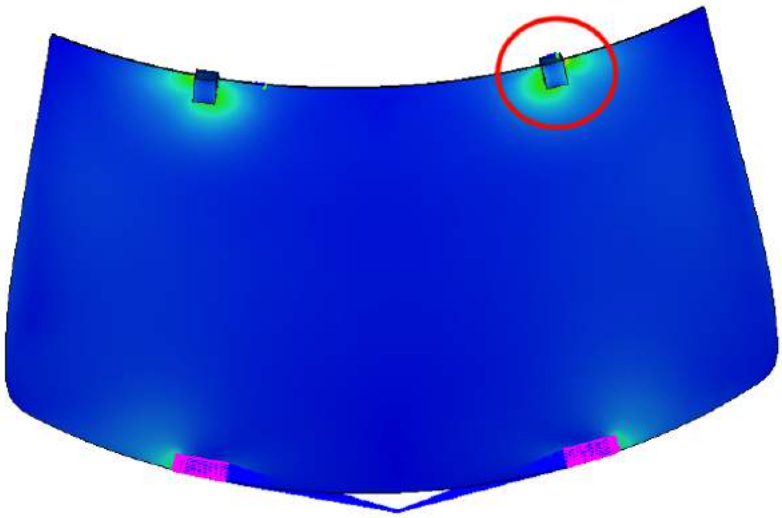

Figure 4.15: Von-mises principle stress- σ_1, Top right spacer

The FE model was validated with the experiment by measuring the stress at areas by selecting the elements and nodes at the same location as at of the gauge from the experiment, see figure 3.20 at a distance of one centimeter from the top right spacer. The node studied here is numbered N302686. The stress rates from the static state and dynamic response have the units of MPa, which is the same unit the validation. The initial static state stress of the windscreen in the rack measured a pre-stress rate close up to 6.5 MPa seen in figure 4.16. It can also be observed from figure 4.16, that the FE model predicts a higher stress of 40 MPa when simulated for static loading, this stress result was further investigated. It was found that the prediction of such high stress was attributed to mesh singularities occurring on the metal bracket and so the high stress prediction was discarded.

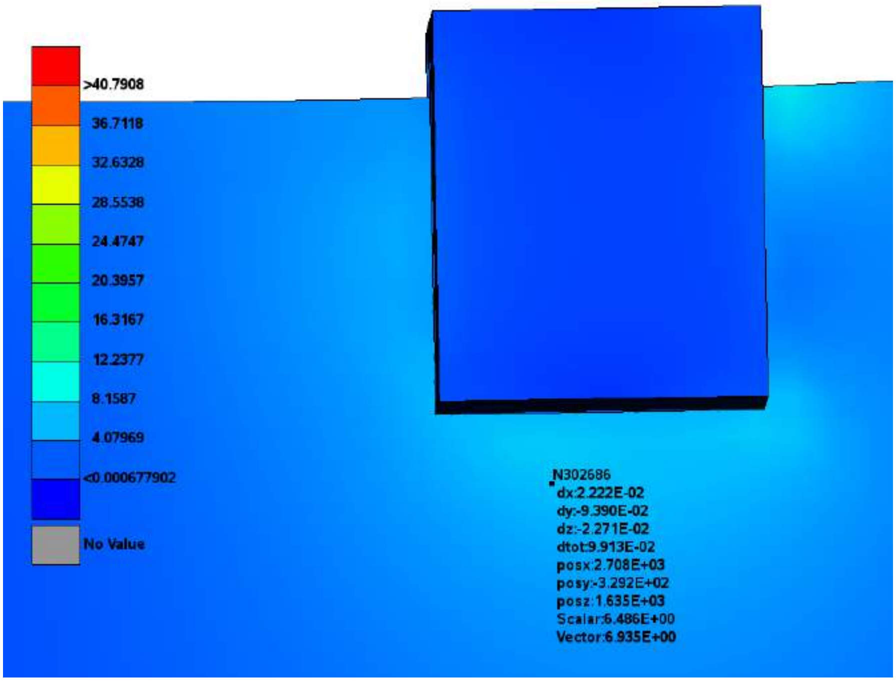

Figure 4.16: Maximum principle stress σ_1 at gauges $2^{3.20}$

The stress state induced during random response is however predicted to have a RMS stress value of 14 MPa measured at the same area as in the static stress state, see figure 4.17. The analytical calculations done using experimental data and substituting the strain response in equation 4.1, calculates the stress state also to be around 14 Mpa. Both figures 4.16 and for 4.17 defines the single real number of stress for the reference nodes with the title “Scalar. The figures are demonstrates the defined data achieved from the specific node(s) in the directions of X, Y Z. The Scalar measurements have the unit MPa, both for static and random response.

The following stress validates that a identical result has been achieved between the FE model and the analytic calculation. By assuring the region, random vibration state, obtained a validation with equation 4.1 are two additional nodes (N294479 and N264231) visualizing the stress distribution of the region and its reliability. The region of the sensor among of the three node references measures all a RMS stress of 14 MPa. It is observed from the figure that the stress state is distributed over a significant area.

Figure 4.17: Maximum principle RMS stress σ_1

Observing the plots of random vibration simulation show a high stress rate at the top of the top right spacer see figure 4.15

In random vibration analysis, the maximum stress achieved state was calculated close to 26 MPa, this is however the RMS value of, vonMises stress in the structure. It is shown in figure 4.18 and was located close to the spacer previously studied in the validation processes. It can be observed that the spacers transfer most of the stress onto the windscreen structure resulting in the spacers being represented in colour 'blue' indicating lower stress values. Figure 4.18 gives an comprehensive overview of the stress distribution. To numerically show the state of stress a node, N287248 is selected during post processing and the stress in this area is measured to be around 26 MPa. This area is depicted by the colour 'red' in the figure. As the area around the spacer experienced a stress of 26 MPa during random vibration, the same area was measured during static loading and resulted in a stress of 9 MPa and is shown in figure 4.19. In this picture, the colours have also changed comparable to the vibration state. The highest areas of stress have now represented by turquoise colour while the rest of the structure remain in blue colour recording very low stress . It is evident from the comparison that even with the change in loading conditions, the area close to the top right spacer is predicted to having higher stress in the structure.

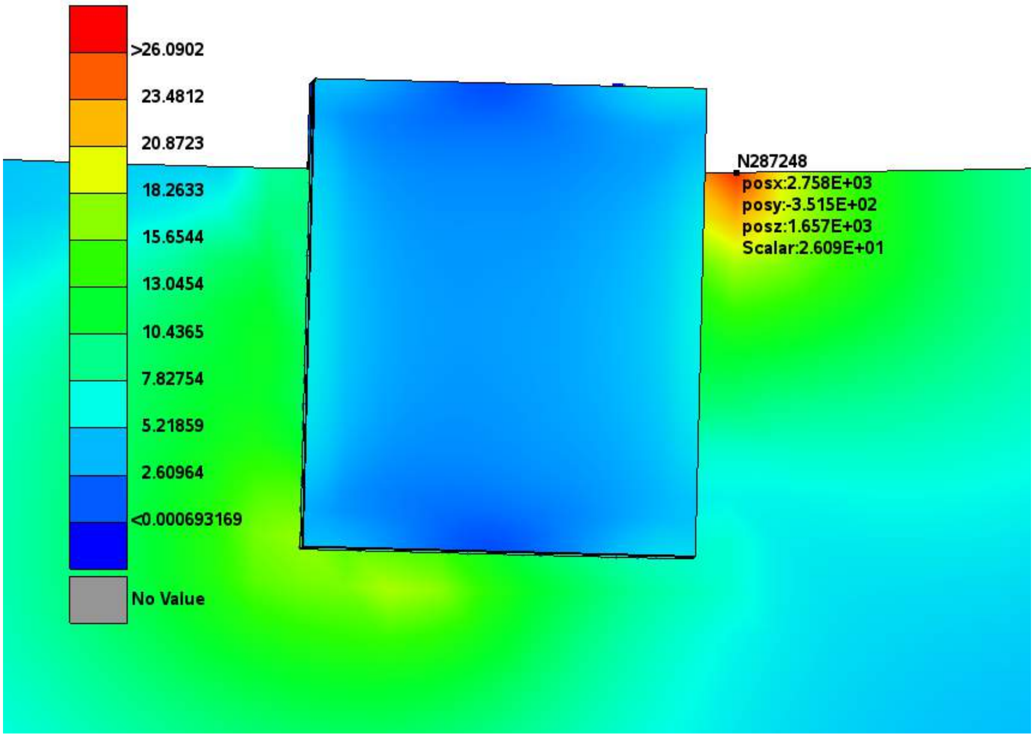

Figure 4.18: The critical stress area location- Random vibration load case

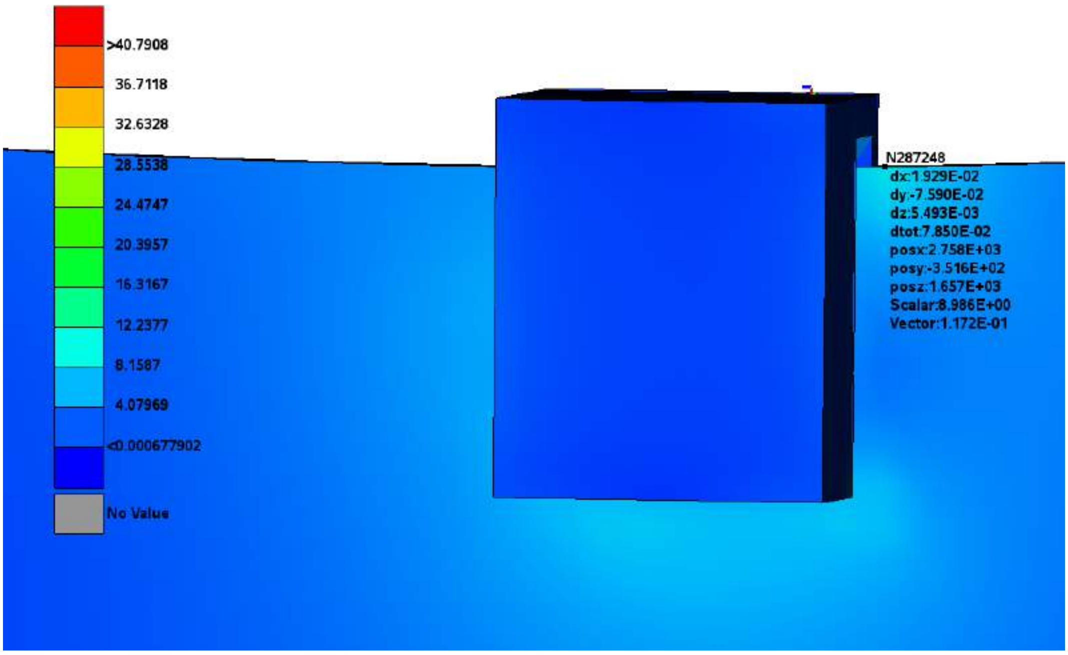

Figure 4.19: Maximum principle stress σ_1- Static load case

5

Conclusion and Discussion

5.1 Discussion of Method

The adopted approach of this thesis was to understanding and predict the dynamic response characteristics and stress states experienced by the windscreens during transportation. Accomplishing the desired objective for VCC required an understanding of the modal response and the random vibration response of the structure. This is achieved by constructing a numerical model of the windscreen structure and simulating it for random response.
The first phase of this methodology, modal analysis, was carried in order to understand the dynamic behavior and to calibrate the material parameters of the windscreen laminate. The methodology thus used was based on iterative calibration [4] and the modal response obtained was similar to results from literature [24]. Thus by studying previous academic reports in the relevant area of research, and validating the FE results with the experimental data a comprehensive overview of the dynamic response of the system and the influence of material properties on these responses were studied . This method was thus implemented onto the constructed numerical model. However, the Experimental Modal Experiment was bounded by equipment and measurement limitations. All necessary equipment and measurement kits for the experiment was provided by VCC, the methodology of the experiment was determined by the factors stated and the work flow was discussed and implemented. The described methodology for both numerical and experimental modal analysis can be replicated and identical results can be obtained.

Having carried out modal analysis, which was used identify and optimize the material parameters of the numerical model, the methodology for accomplishing random vibration was established. Here, random vibration is used to simulate the truck vibration experienced by the windscreens during transportation. With limitations on the availability of vibration rigs at VCC, the random vibration experiment was carried out at RISE, Borås. The input PSD used to simulate random vibration was setup according to ASTM D4169-16 DC3 which is a truck vibration standard used in the prediction of random responses of packages and goods which are transported for long distances. This standard was selected as it was the most apt for the transport case of windscreens, with higher energies at the lower frequencies which more so is the case. The authors did face some limitations with this approach as the vibration test rig was unable to excite the windscreen setup at frequencies above 30Hz due to the weight restrictions. It can be said that, the followed methodology was not

successful in validating the numerical stresses results due to this limitation. The restrictions of control and safety regulations, could not a response signal from a loaded truck be simulated with the transportation rack. Therefore, was the ASTM standard a realistic alternative considered, in order to simulate the FE-model with a PSD-load. Unfortunately higher frequencies could not be simulated at RISE, due to the test shaker table's limitation with respect to the mass and volume of the rack. Forming the measuring on a truck during delivery would have been the best option of studying the road condition and the complete transportation distance with a full rack, 37 windscreens. The benefits of the simulations were by allowing re positioning sampling order and studying the impact depending of the positioning inside the rack. Following experiments gave the authors the knowledge of how positioning and the acting forces of the surrounding is affecting in following situation. The gauges, placed at the windscreen, were selected at areas with amplified mass displacement than areas with close to supports. It was also found out that those areas had considerably lower stress rate than the areas close to the supports. The variations of stress between areas were unknown and tested in this experiment as a result for future studies.
The selection of methods was exceptional for the work and made it possible of accomplishing the desired objective. The methodologies in this work were new areas of learning previously unknown by the authors. Following work has contributed in advantage knowledge within the field of work for both the authors and the VCC for future projects. To be part of Exterior Glass Group team and learning how to professional handling challenges and developing solutions have been extremely rewarding for the both authors.

5.2 Discussion of Results

The previous section discussed the methodology selection with the following section discussing the results obtained by applying the set methodology.

As the work is structured as a research project, the work is bound by limitations, which effect the accuracy of the obtained result. For instance, the plastic interlayer is in general a viscoelastic material, but in the constructed numerical model the plastic interlayer is modeled as a linear material. In doing so, the interlayer does not exhibit any viscoelastic material behaviour, this assumption of a linear behaviour leads to a simplified model. The method of iterative calibration adopted during this work limits the applicability of the material card for applications to development of windscreens at lower range of frequency values as the method was not successful in predicting validated behavior at frequency range above 100Hz. This can however be improved upon by developing a viscoelastic material model for the PVB interlayer. The simplification of the model as a linear elastic model is however predicted to have an effect on the stress distribution. As a visco eleastic model will have both time dependent and frequency dependent behaviour, negating it will have a higher impact on the stress results at higher frequencies. This assumption also adds in the fact that the numerical model predicts linear distribution of stress through the thickness which seldom is the case. The setup of this work with provided facilities and soft-

ware would not have affected the outcome of results achieved. If another company would carry out the similar experiment, they should achieve similar results as the experimentation and the validation of the numerical model is carried out according to ASTM and industry standards. The working procedure setup during the course of work can be replicated which will yield identical results. The software used was well known in this field of work, and what might have difference is the procedure between the software's codes it is written. VCC, had limited facilities to carry out the random vibration, and therefore the experiment was carried out at RISE, Borås which provided the authors with the facilities to perform the experiment. The ideal case for authors would have been to carry out a physical experiment up to 100 Hz instead the frequency range was limited to 30 Hz, due to the weight restrictions of the specimen that could be mounted on the vibration rig. If the entire spectrum of 100 Hz could have been simulated, the authors believe that more data points to validate the numerical model could have been achieved which in turn would have helped in a better validation of the stress distribution predicted by the numerical model. The positioning of the windscreen in the rack created a variance of stress distribution. All windscreens were not affected by the same stress. The positioning in the rack decided the distribution of stress. All the boundary conditions and constraints were in terms with the packaging directions setup by VCC. The only variance was the application of the rear load on the windscreen, which is an effect of consecutive windscreens resting on each other. This force is a function of the assumed angle see appendix D. Thus a variation in this resting angle provides varied forces which have its impact on the predicted stress distribution. It is also observed that the windscreens positioned closest to the rack's supports would have a higher affect of stress than the windscreens away from the supports. This was because of the weight from the windscreens as they are resting on each other. If another packaging design were applied, which eliminates the tilting weight of the windscreens, could eliminate the variance among the windscreens.
The investigated results have given VCC a better understanding and an insight of the truck transportation of windscreens with their current packaging orientation for truck transportation. The findings can be useful tools for future development of new products as both cost and time savings.

5.3 Conclusion

The conclusions of the findings and results for this master thesis work will be presented in this section in terms of bullet points to highlight the main accomplishes of this work.

- The most suitable realistic element structure mimicking a laminate was a solid hexa structure element and its evenly distribution, which cannot be made the same for tetras.
- The mode shapes from both the EMA and the FE-simulation were well correlated
- A material card with updated properties for glass as polyvinyl was identified and validated against the experimental modal analysis

- The numerical windscreen had corresponding results with the dynamic stress experiment
- The static state stress begin at 6 MPa and with random vibration the stress increased to 14 MPa (1 cm below the spacer)
- The critical area close to the spacer had static state stress at 14 MPa and with random vibration stress 26 MPa, close to the tensile strength of glass

The following work has provided VCC with a functional numerical model with documentation of stresses for one of their car models in both a static and vibration state. The following methodology procedure was shown to be successful for the following investigations and similar process can be used for other studies.

6

Future Recommendations

This chapter presents possible future investigations or recommendations for further improving the FE-model and the experimental results.

The laminate structure in this study was modelled as a linear material for all layers, the approach of considering all layers as linear is carried in order to simplify of the construction and the validation of geometry. The model can be updated with a viscoelastic inter layer in order to predict the time dependent and frequency dependency on the laminate with higher accuracy.

In the work of experimental modal analysis, impact hammer was used for exciting the windscreen at the marked points. What is recommended for further studies is to use a shaker excitation instead and compare the result with the carried out experiment. A shaker can provide with richer energy rate to the structure for a longer period of time while for an impact hammer the response time is limited. A shaker as the ability to provide a better control over the frequency range of interest is selected by the shaker.

Fatigue testing is highly recommended for the complete transportation distance from supplier to factory, this is to predict how the stress affect the quality of the windscreen. If the critical area close to the spacer tends to be true, the next procedure is to study new possible packaging solutions.

To lower the stress rate, one of the parameter that can be varied and studied is the different packaging orientations, It is evident from previous and the current study that the constraints in the packaging having a very high impact on the distribution of stresses on the windscreens. Hence, if new packaging orientations are proposed, it makes it vital to have a parameter study on the different packaging orientation in order to understand and predict the distribution of stresses when it is exposed to random vibrations.

To simulate a realistic connections between the spacers and the windscreens can be numerically constructed as sliding contacts rather than rigid body contacts which will help in a better distribution of stresses at the predicted critical areas. So a parameter study on the contacts used is recommended.

Another interesting investigation is how the laminate curvature of the windscreen affects the stress results. A curvature study would be an interesting investigation to see if the stress rate is affected by the curvature.

The final recommendation given is to perform a parameter study with different windscreens models and shapes, to investigate if the behavior as stress rate is maintained or similar to the achieved results.

Bibliography

[1] Volvo Car Corporation, "https://group.volvocars.com/company= "(accessed: 07.05.2018)".

[2] VCC (2017) *Windscreen stacking and packaging manual*, Internal Document, Unpublished.

[3] VCC (2018) *Design of Windscreens,* Internal Document, Unpublished.

[4] VCC (2017) *Modal analysis and material parameter optimization for windscreens*, Internal Document, Unpublished

[5] Barry Controls, Hopkinton, MA .*Random Vibration- An Overview.* Available from: http://www.emtengineering.com [Accessed: 04.28.2018].

[6] Gerrit Visser (2014), *Modal Analysis: What it is an dis not.* Available from: https://esteq.co.za/2014/11/25/modal/ [Accessed: 03.20.2018].

[7] Brandt, A. (2010). Noise and Vibration Analysis: Signal Analysis and Experimental Procedures. John Wiley Sons, New York, NY, USA

[8] CHOPRA, A. K. (2007). *Dynamics of structures: theory and applications to earthquake engineering.* Englewood Cliffs, N.J., Prentice Hall.

[9] Siemens 2018 PLM, Siemens PLM Community. *Siemens PLM Community: What is a Frequency Response Function (FRF)?* Available from: https://community.plm.automation.siemens.com/t5/Testing-Knowledge-Base/What-is-a-Frequency-Response-Function-FRF/ta-p/354778 [accessed: 03.31.2018]

[10] Bülah, K Yusuf and Scanlan, Robert H.(1991) Resonance, Tacoma Narrows bridge failure, and undergraduate physics textbooks. *American Journal of Physics* 59, 118. Available from: https://aapt.scitation.org/doi/10.1119/1.16590

[11] Roland Priemer (1991). *Advanced Series in Electrical and Computer Engineering: Introductory Signal Processing*, World Scientific Publishing.

[12] Agilent Technologies. *The Fundamentals of Signal Analysis: Application Note 24* Available from: http://www.modalshop.com/techlibrary [accessed: 03.31.2018]

[13] Allaby, Michael (2013). *A dictionary of geology and earth sciences*, Oxford University Press.

[14] Ridpath, Ian,(2012). *A dictionary of astronomy*, Oxford University Press.

[15] Logan, Daryl .L (2011). *A first course in the finite element method*, Cengage Learning.

[16] Scigliano, R and Scionti, M and Lardeur, P (2011) , Verification, validation and variability for the vibration study of a car windscreen modeled by finite elements *Finite Elements in Analysis and Design* 47, 17-29.

[17] Banwell, Guy and Mohr, Stefan and Rothberg, Steve and Roberts, Jon (2012), Using experimental modal analysis to validate a finite element model of a tennis racket *Procedia Engineering* 34, 688–693.

[18] Peter Hansbo (2006). *Non-linear Finite Element Analysis Advanced topics.*

[19] WESTPACK, INC. *ASTM D4169-16 Truck Vibration Changes* Available from: https://www.westpak.com [accessed: 04.22.2018].

[20] Jarimopas, Bundit and Singh, S.Paul and Saengnil, Wasan (2005), Measurment and Analysis of Truck Transport Vibration Levels and Damage to Packaged Tangerines during Transit, *PACKAGING, TECHNOLOGY AND SCIENCE* 18, 179–188.

[21] Berardinelli, A. and Donati, A. and Giunchi, A. and Ragni, L. (2003), Effects of Transport Vibration on Quality Indices of Shell Eggs' *Biosystems Engineering*, 86, 495–502.

[22] RISE Research Institues of Sweden, *Accelerating Innovation*, Available from: https://www.ri.se/en [accessed on: 04.22.2018].

[23] Mikael Helgesson (2015) *Response of a rocket nozzle to power spectral density loads.* Master Thesis. Luleå University of Technology, Sweden.

[24] Karl Johan Larsson, Snaevar LeoGretarsson, Majid K. Vakilzadeh and Thomas Abrahamsson.*Calibration and Cross-Validation of a Car Component Model using Repeated Testing.* Chalmers University of Technology, Sweden.

[25] Özgür BAYRAKDAR (2010) *Random Vibration of a Road Vehicle*. Master Thesis. İzmir Institute of Technology, Turkey.

[26] Ye Lu (2013) *Comparison of Finite Element Method and Modal Analysis of Violin Top Plate*. Master Thesis. McGill University. Montreal, Canada.

[27] Camilla Fors (2014) *Mechanical Properties of Interlayers in Laminated Glass*. Master Thesis. Lund University. Sweden.

[28] Maria Froling (2011) *Strength and Design Methods for Laminated Glass*. Licentiate Dissertation. Lund University, Sweden.

[29] Gergely Molnar, Laszlo Gergely Vigh, Gyorgy Stocker, Laszlo Dunai (2012), Finite Element analysis of laminated structural glass plates with polyvinyl butyral (PVB) interlayer.*Periodica Polytechnica* 56/1, 35–42.

[30] Jun Xu, Yibing Li, Bohan Liu, Mengyi Zhu, Dongyun Ge (2011), Experimental study on the mechanical behaviour of PVB laminated glass under quasi-static and dynamic loadings, *Composites: Part B* 42, 302–308. Avalilabe on : https://www.elsevier.com/locate/compositesb [accessed: 04.22.2018].

[31] Ahmet Levent Avsar (2008).*Dynamic Modelling and Analysis of Vibration Effects on Performance in Optical Systems*. Master Thesis. The Graduate School of Natural and Applied Sciences of Middle Eaast Technical University

[32] Predictive Engineering (2014). *Principals of Vibration Analysis: Normal Modes to PSD to Direct Transient*. Available from: https://www.predictiveengineering.com [Accessed 04.25.2015].

[33] S.K Thampi, S.N Vidyasagar. *Random Vibration Analysis of Space Flight Hardware using Nastran*. Available from: https://ntrs.nasa.gov [Accessed 04.25.2018].

[34] *Performing a Random Vibration (PSD) Analysis*. Available from:https://www.sharcnet.ca/Software/Ansys/16.2.3/en-us/help/ans_str/Hlp_G_STR6_8.html [Accessed 04.27.2018].

[35] Beta Simulation Solutions *Manual: Ansa pre-processor*. 2017.

[36] Beta Simulation Solutions *Manual: Meta post-processor*. 2017.

[37] MSC Software *MSC Nastran*.2017.

[38] RISE *Transport Vibration Test of a Transportation Rack with Windscreens*, Volvo Car Corporation, Internal Document, Unpublished.

A
Appendix- Mode Shapes

Phase 1

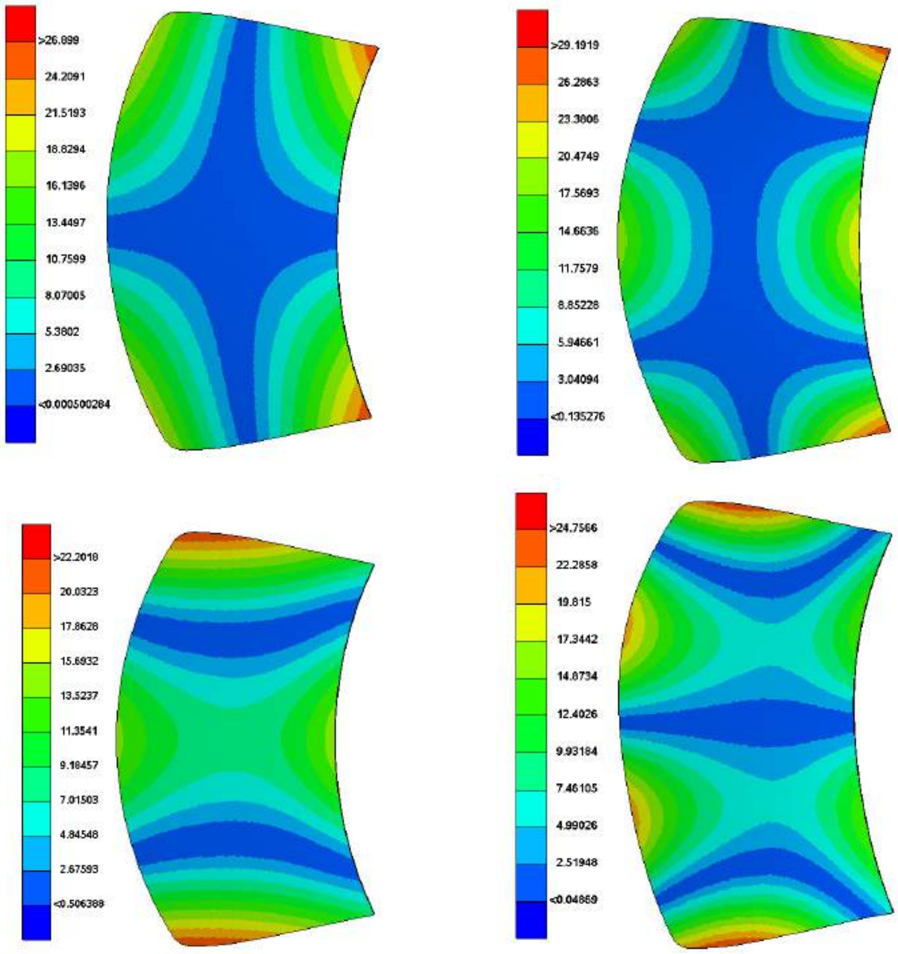

Mode 1

Mode 3

Mode 2

Mode 4

Phase 1

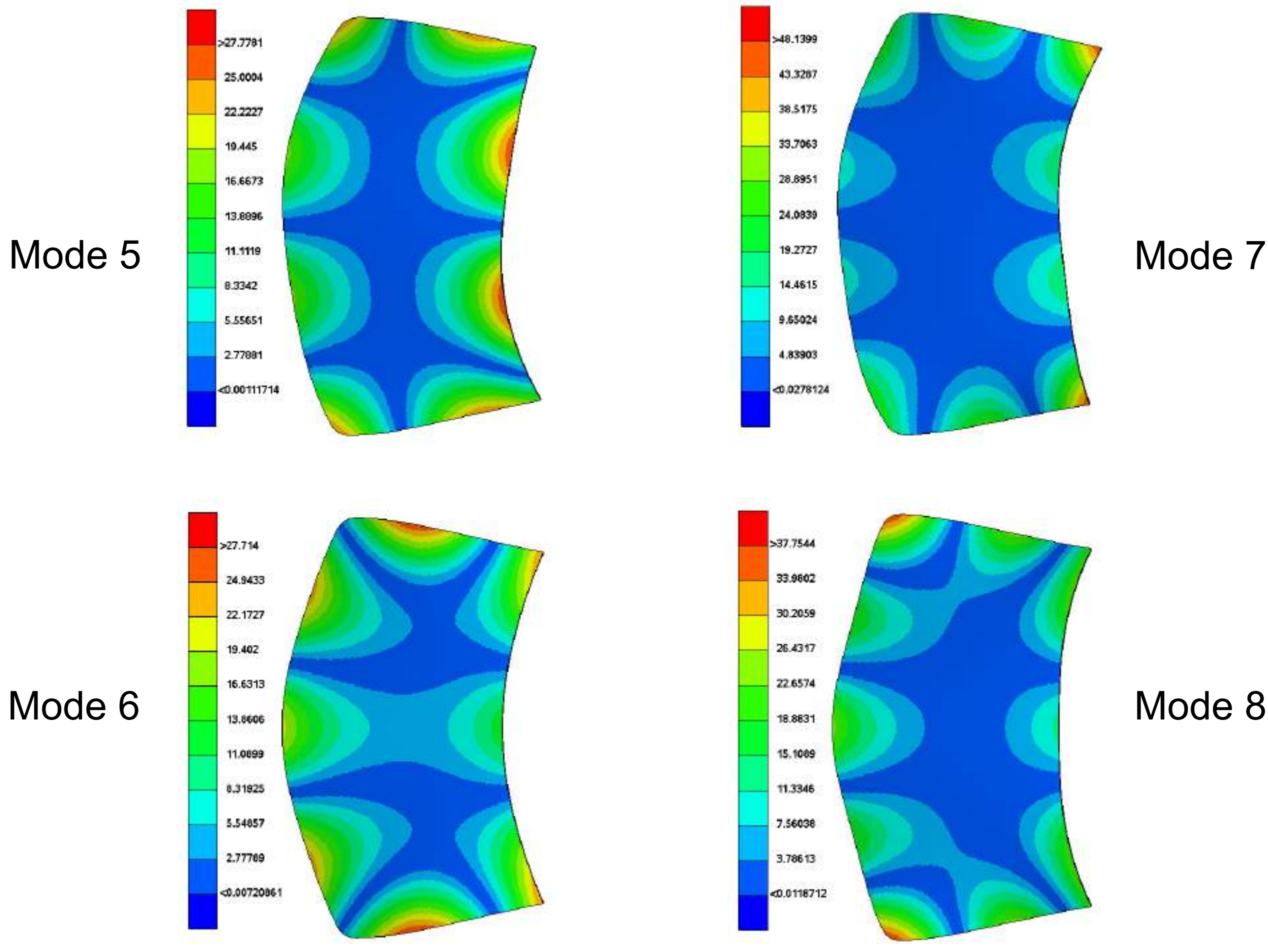
Mode 5
>27.7781
25.0004
22.2227
19.445
16.6673
13.8896
11.1119
8.3342
5.55651
2.77881
<0.00111714
Mode 7
>48.1399
43.3287
38.5175
33.7063
28.8951
24.0839
19.2727
14.4615
9.65024
4.83903
<0.0278124
Mode 6
>27.714
24.9433
22.1727
19.402
16.6313
13.8606
11.0899
8.31925
5.54857
2.77789
<0.00720861
Mode 8
>37.7544
33.9802
30.2059
26.4317
22.6574
18.8831
15.1089
11.3346
7.56038
3.78613
<0.0118712

Phase 1

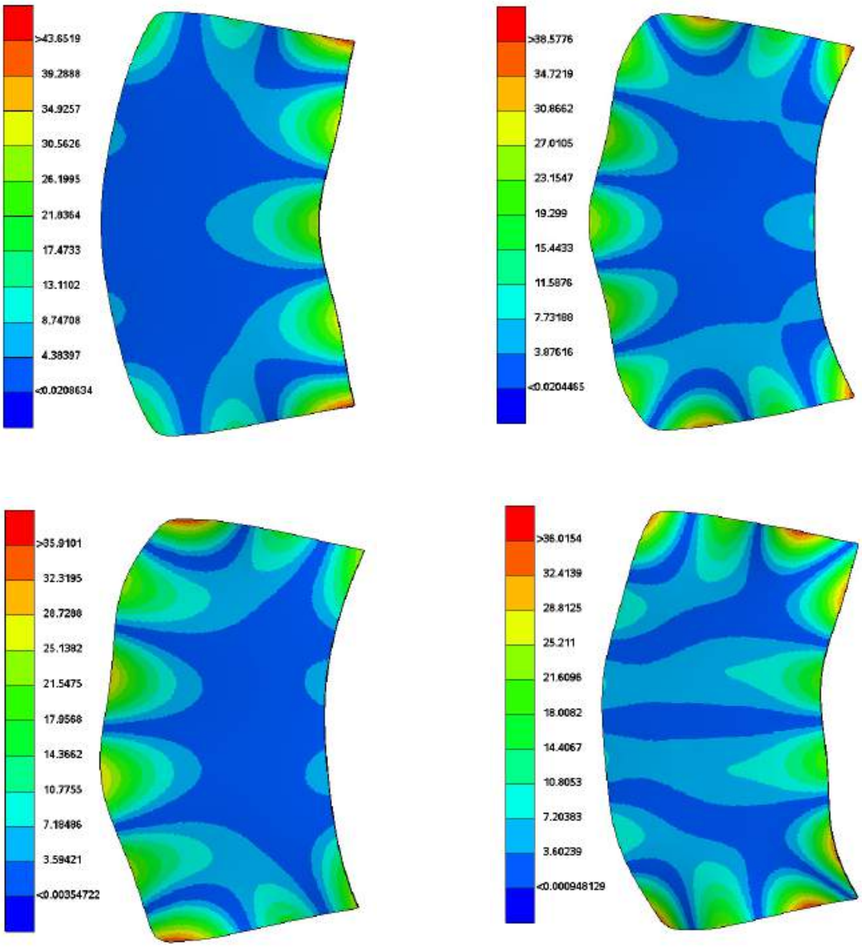

Mode 9

Mode 11

Mode 10

Mode 12

Phase 1

Mode 13

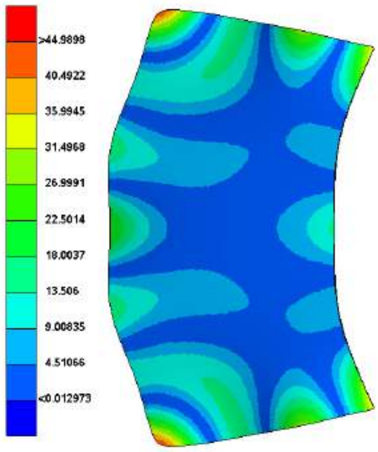

Mode 14

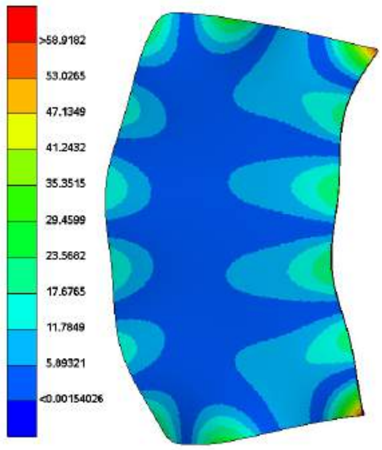

Phase 2

Mode 1

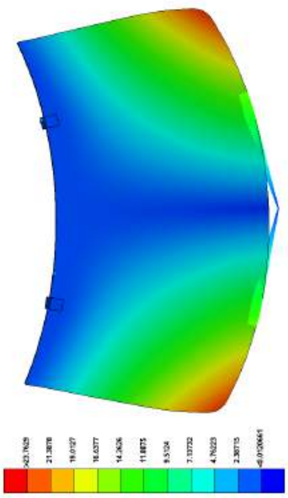

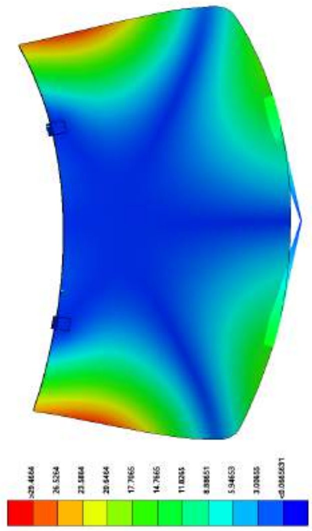

Mode 3

Mode 2

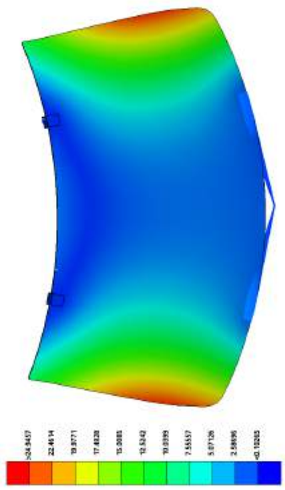

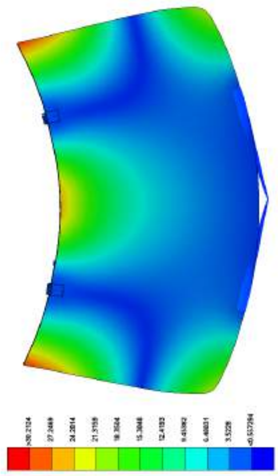

Mode 4

Phase 2

Mode 5

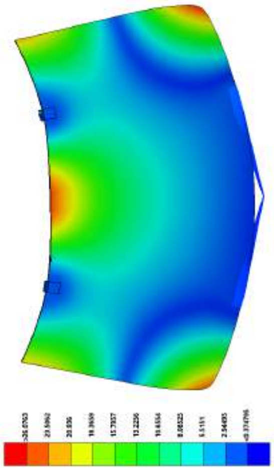

Mode 7

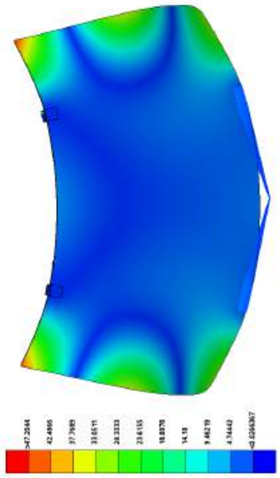

Mode 6

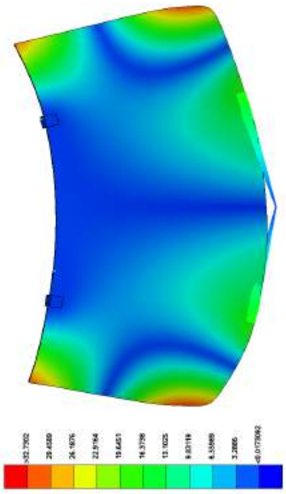

Mode 8

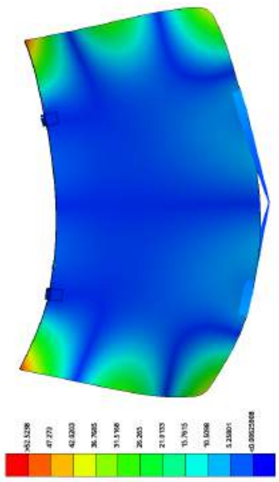

Phase 2

Mode 9

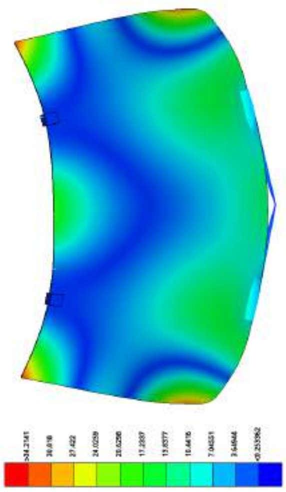

Mode 11

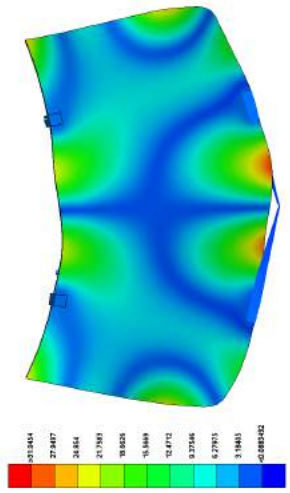

Mode 10

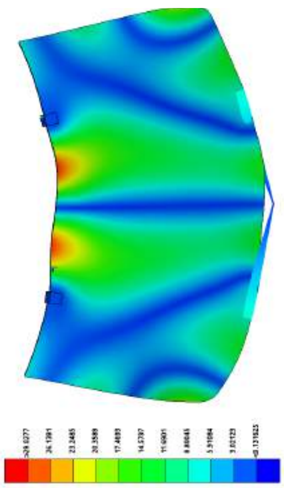

Mode 12

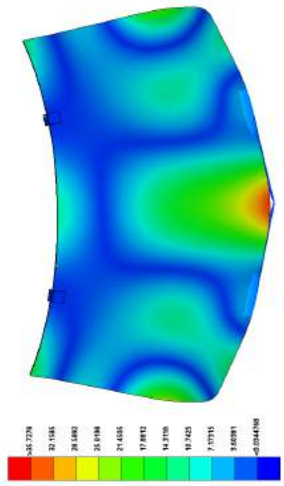

Phase 2

Mode 13

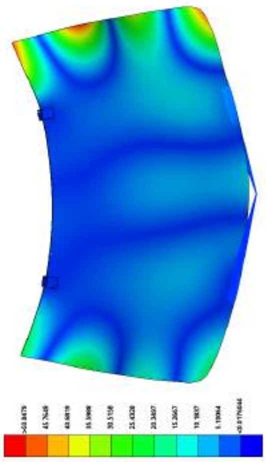

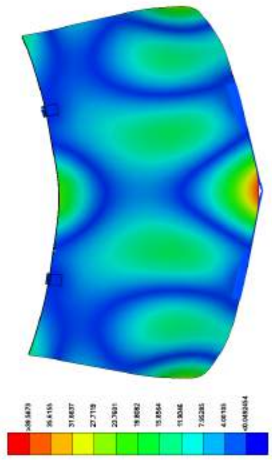

Mode 15

Mode 14

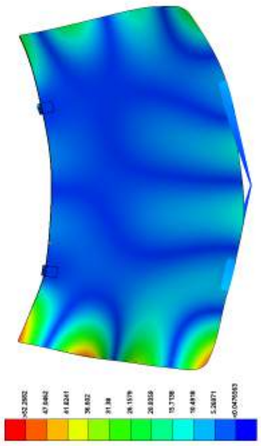

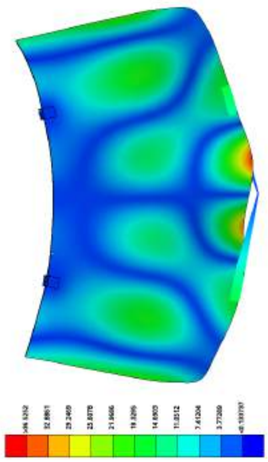

Mode 16

Phase 2

Mode 17

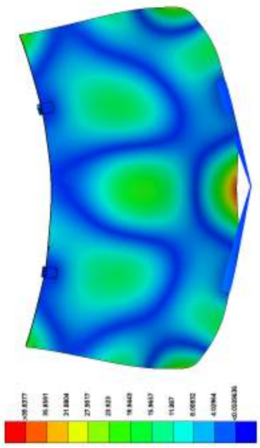

Mode 19

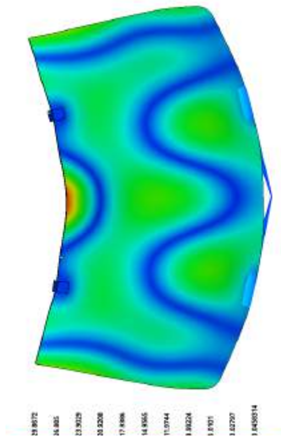

Mode 18

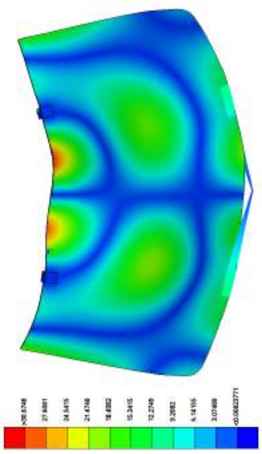

Mode 20

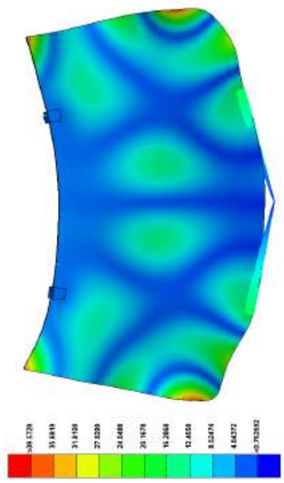

B

Appendix- Response Strain PSD

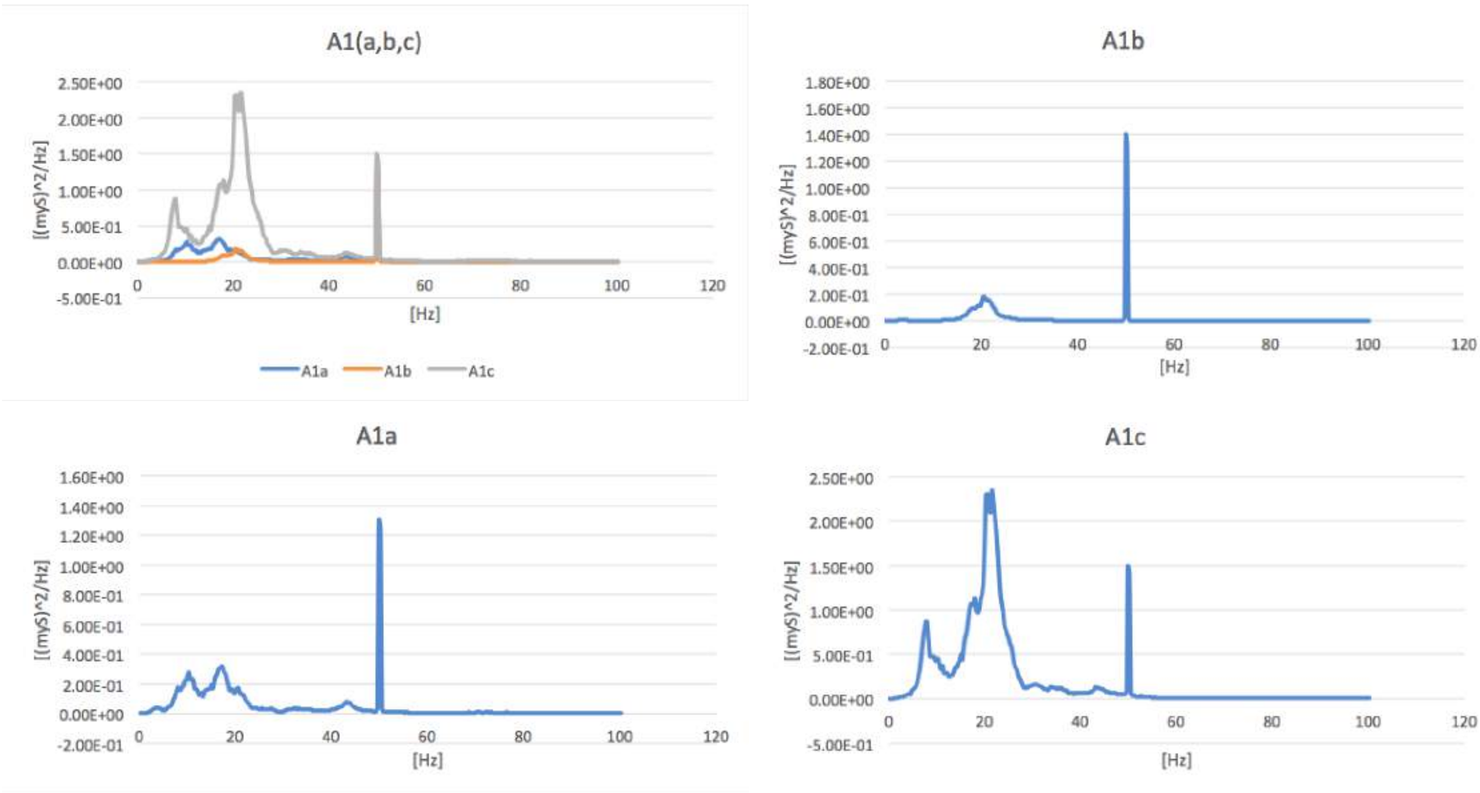
A1(a,b,c)
2.50E+00
2.00E+00
1.50E+00
1.00E+00
5.00E-01
0.00E+00
-5.00E-01
[(myS)^2/Hz]
0
20
40
60
80
100
120
[Hz]
A1a
A1b
A1c
A1b
1.80E+00
1.60E+00
1.40E+00
1.20E+00
1.00E+00
8.00E-01
6.00E-01
4.00E-01
2.00E-01
0.00E+00
-2.00E-01
[(myS)^2/Hz]
[Hz]
A1a
1.60E+00
1.40E+00
1.20E+00
1.00E+00
8.00E-01
6.00E-01
4.00E-01
2.00E-01
0.00E+00
-2.00E-01
[(myS)^2/Hz]
[Hz]
A1c
2.50E+00
2.00E+00
1.50E+00
1.00E+00
5.00E-01
0.00E+00
-5.00E-01
[(myS)^2/Hz]
[Hz]

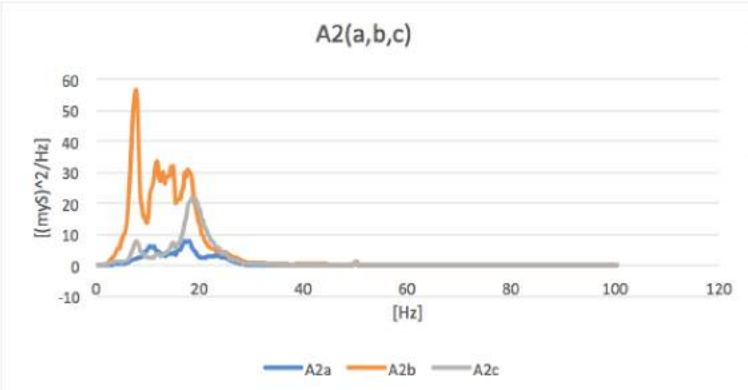
A2(a,b,c)
[(myS)^2/Hz]
[Hz]
A2a
A2b
A2c

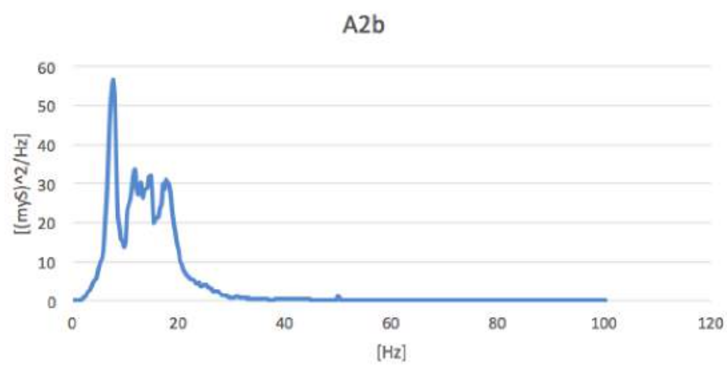
A2b
[(myS)^2/Hz]
[Hz]

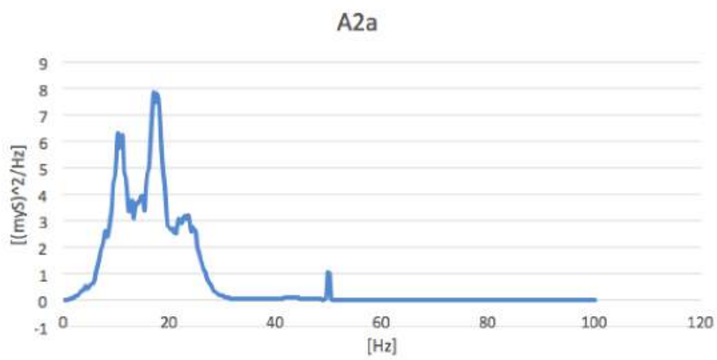
A2a
[(myS)^2/Hz]
[Hz]

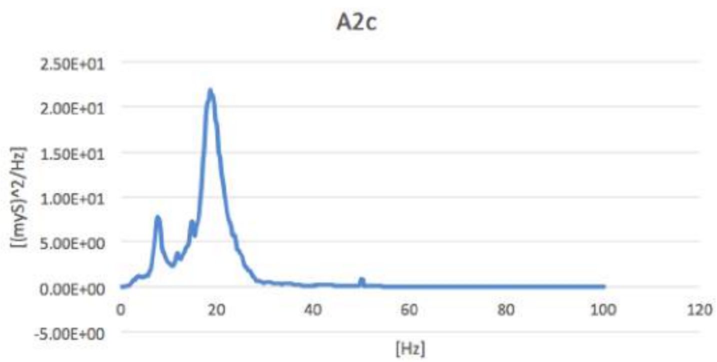
A2c
[(myS)^2/Hz]
[Hz]

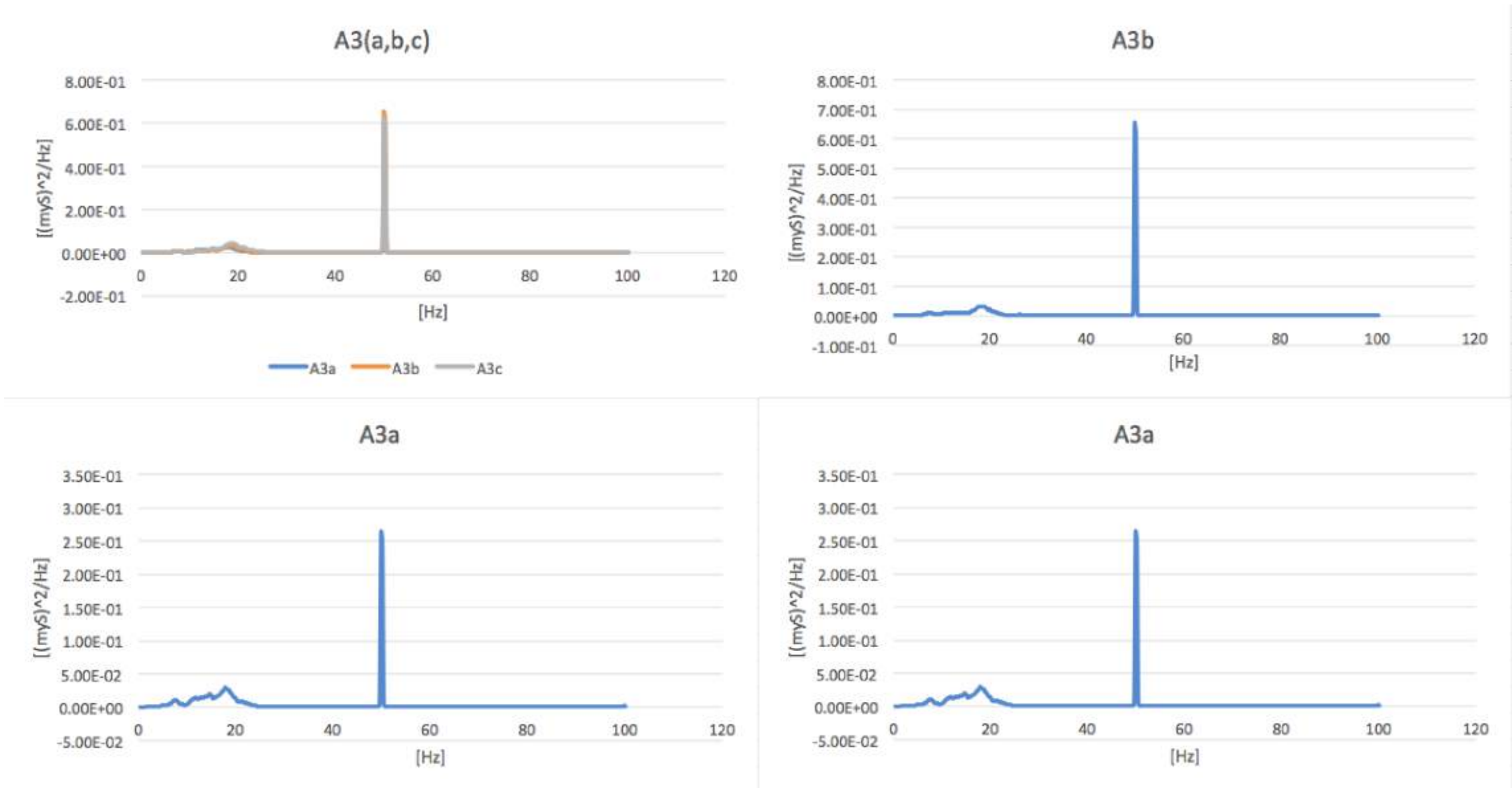
A3(a,b,c)
8.00E-01
6.00E-01
4.00E-01
2.00E-01
0.00E+00
-2.00E-01
0
20
40
60
80
100
120
[Hz]
[(my$)^2/Hz]
A3a
A3b
A3c
A3b
8.00E-01
7.00E-01
6.00E-01
5.00E-01
4.00E-01
3.00E-01
2.00E-01
1.00E-01
0.00E+00
-1.00E-01
[(my$)^2/Hz]
[Hz]
A3a
3.50E-01
3.00E-01
2.50E-01
2.00E-01
1.50E-01
1.00E-01
5.00E-02
0.00E+00
-5.00E-02
[(my$)^2/Hz]
[Hz]
A3a
[(my$)^2/Hz]
[Hz]

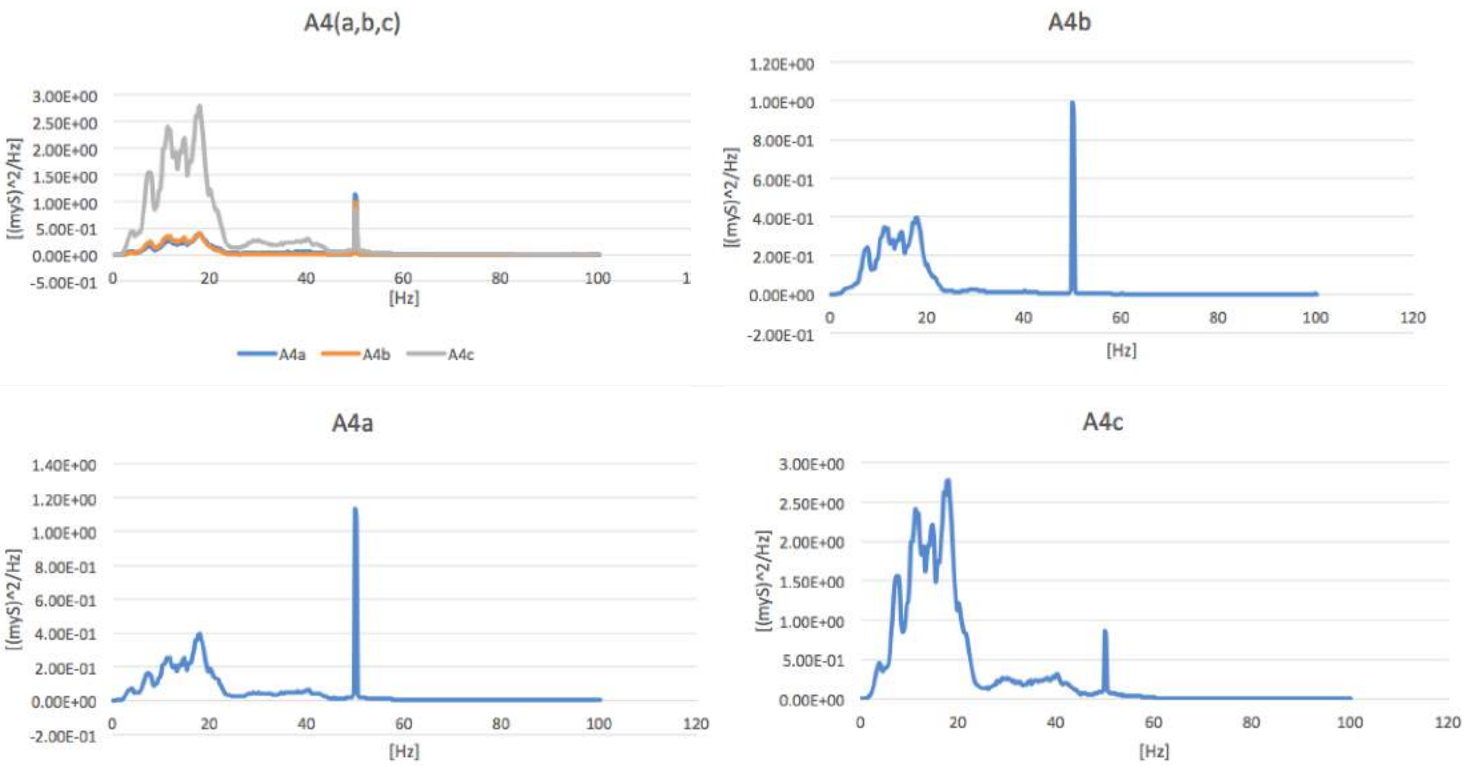
A4(a,b,c)
[(myS)^2/Hz]
[Hz]
A4a
A4b
A4c
A4b
[(myS)^2/Hz]
[Hz]
A4a
[(myS)^2/Hz]
[Hz]
A4c
[(myS)^2/Hz]
[Hz]

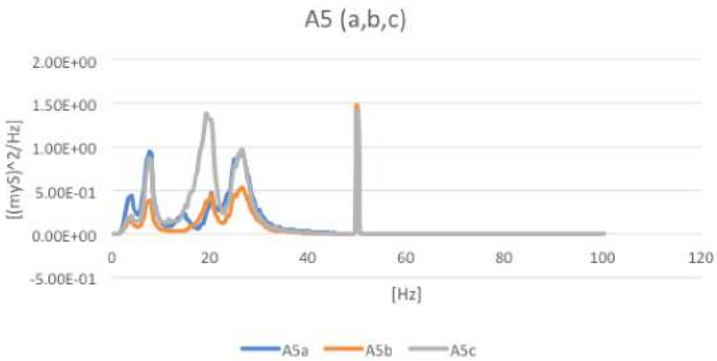
A5 (a,b,c)
2.00E+00
1.50E+00
1.00E+00
5.00E-01
0.00E+00
-5.00E-01
[(myS)^2/Hz]
0
20
40
60
80
100
120
[Hz]
A5a
A5b
A5c

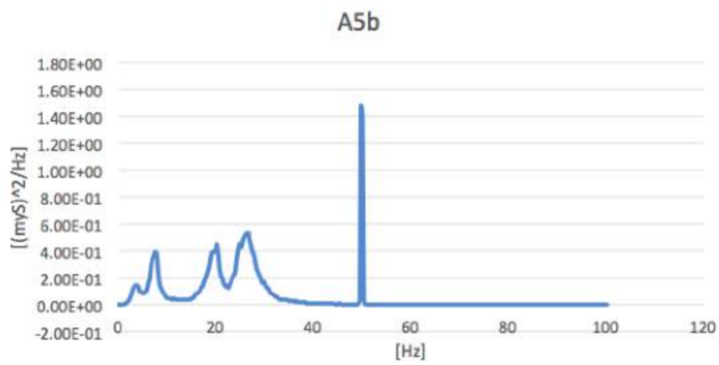
A5b
1.80E+00
1.60E+00
1.40E+00
1.20E+00
1.00E+00
8.00E-01
6.00E-01
4.00E-01
2.00E-01
0.00E+00
-2.00E-01
[(myS)^2/Hz]
0
20
40
60
80
100
120
[Hz]

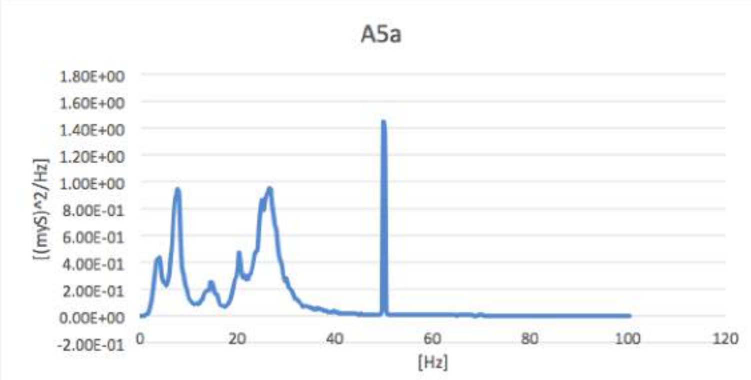
A5a
1.80E+00
1.60E+00
1.40E+00
1.20E+00
1.00E+00
8.00E-01
6.00E-01
4.00E-01
2.00E-01
0.00E+00
-2.00E-01
[(myS)^2/Hz]
0
20
40
60
80
100
120
[Hz]

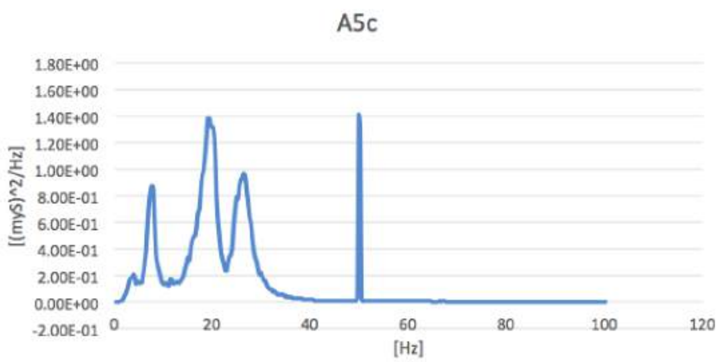
A5c
1.80E+00
1.60E+00
1.40E+00
1.20E+00
1.00E+00
8.00E-01
6.00E-01
4.00E-01
2.00E-01
0.00E+00
-2.00E-01
[(myS)^2/Hz]
0
20
40
60
80
100
120
[Hz]

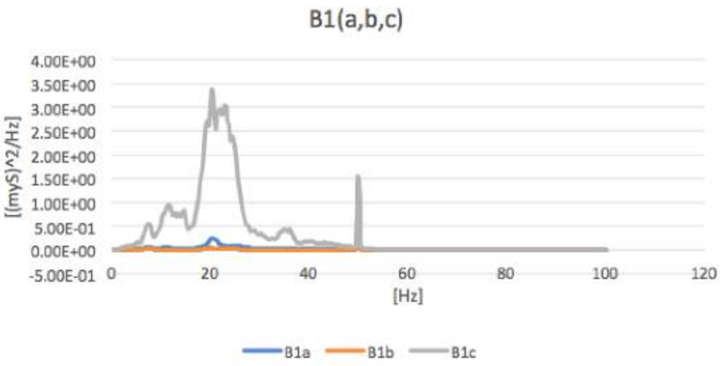
B1(a,b,c)
4.00E+00
3.50E+00
3.00E+00
2.50E+00
2.00E+00
1.50E+00
1.00E+00
5.00E-01
0.00E+00
-5.00E-01
0
20
40
60
80
100
120
[Hz]
[(myS)^2/Hz]
B1a
B1b
B1c

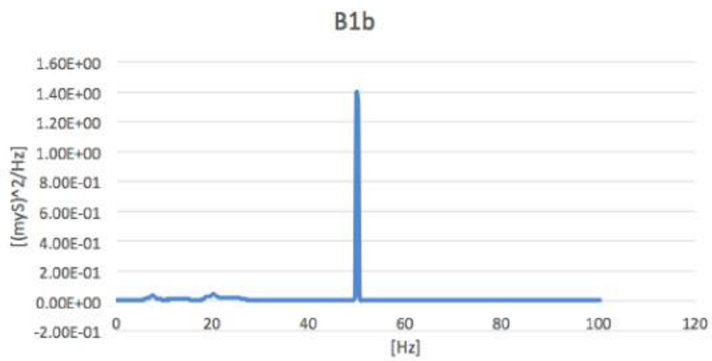
B1b
1.60E+00
1.40E+00
1.20E+00
1.00E+00
8.00E-01
6.00E-01
4.00E-01
2.00E-01
0.00E+00
-2.00E-01
0
20
40
60
80
100
120
[Hz]
[(myS)^2/Hz]

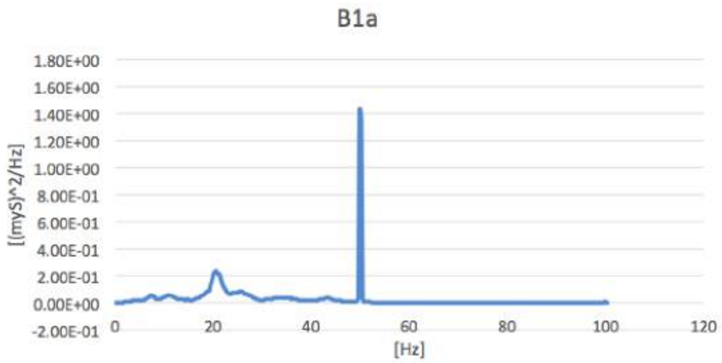
B1a
1.80E+00
1.60E+00
1.40E+00
1.20E+00
1.00E+00
8.00E-01
6.00E-01
4.00E-01
2.00E-01
0.00E+00
-2.00E-01
0
20
40
60
80
100
120
[Hz]
[(myS)^2/Hz]

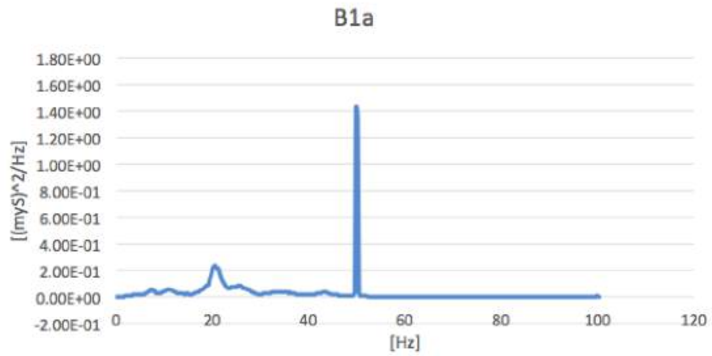
B1a
1.80E+00
1.60E+00
1.40E+00
1.20E+00
1.00E+00
8.00E-01
6.00E-01
4.00E-01
2.00E-01
0.00E+00
-2.00E-01
0
20
40
60
80
100
120
[Hz]
[(myS)^2/Hz]

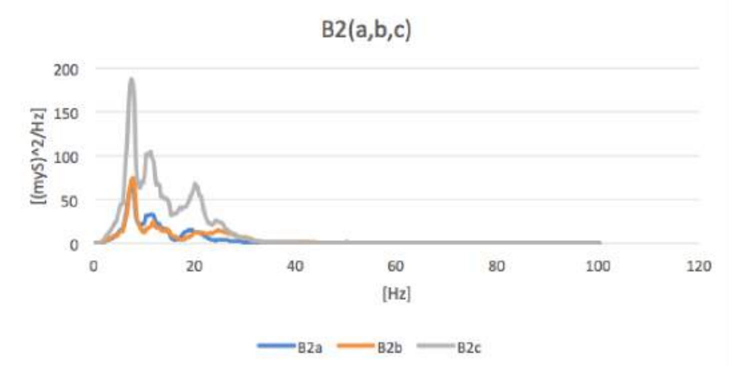
B2(a,b,c)
200
150
100
50
0
[(myS)^2/Hz]
0
20
40
60
80
100
120
[Hz]
B2a
B2b
B2c

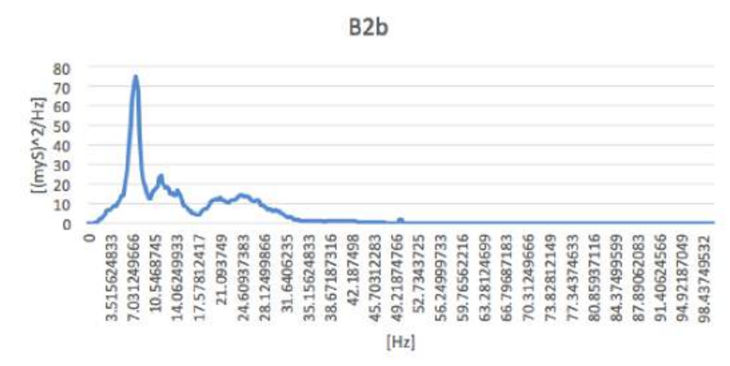
B2b
80
70
60
50
40
30
20
10
0
[(myS)^2/Hz]
0
3.515624833
7.031249666
10.5468745
14.06249933
17.57812417
21.093749
24.60937383
28.12499866
31.6406235
35.15624833
38.67187316
42.187498
45.70312283
49.21874766
52.7343725
56.24999733
59.76562216
63.28124699
66.79687183
70.31249666
73.82812149
77.34374633
80.85937116
84.37499599
87.89062083
91.40624566
94.92187049
98.43749532
[Hz]

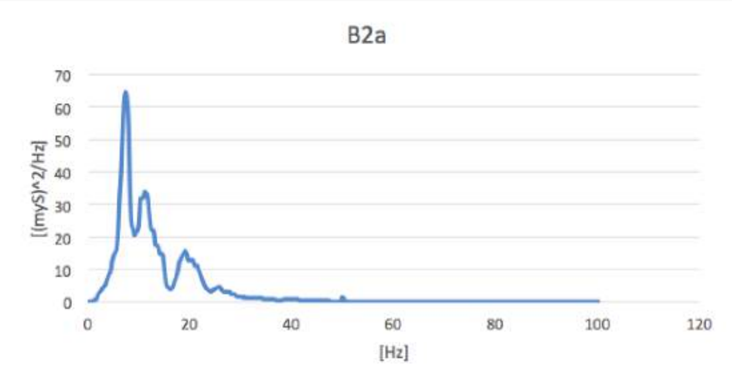
B2a
70
60
50
40
30
20
10
0
[(myS)^2/Hz]
0
20
40
60
80
100
120
[Hz]

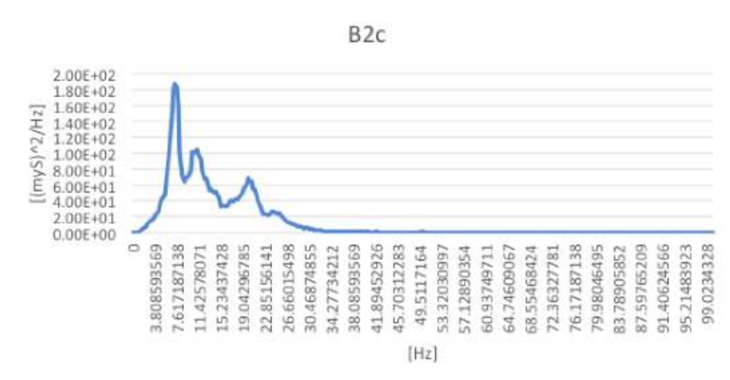
B2c
2.00E+02
1.80E+02
1.60E+02
1.40E+02
1.20E+02
1.00E+02
8.00E+01
6.00E+01
4.00E+01
2.00E+01
0.00E+00
[(myS)^2/Hz]
0
3.808593569
7.617187138
11.42578071
15.23437428
19.04296785
22.85156141
26.66015498
30.46874855
34.27734212
38.08593569
41.89452926
45.70312283
49.5117164
53.32030997
57.12890354
60.93749711
64.74609067
68.55468424
72.36327781
76.17187138
79.98046495
83.78905852
87.59765209
91.40624566
95.21483923
99.0234328
[Hz]

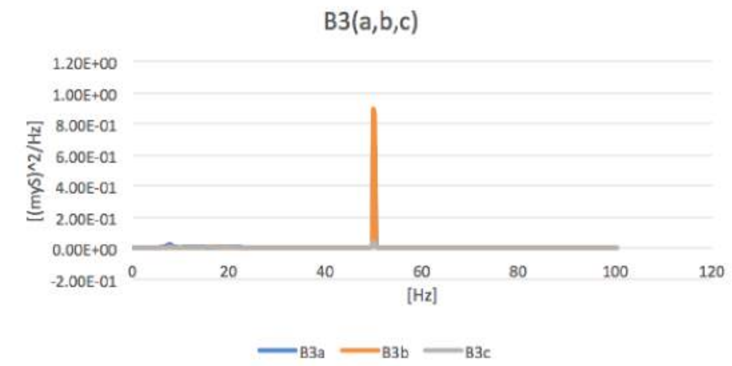

B3(a,b,c)
1.20E+00
1.00E+00
8.00E-01
6.00E-01
4.00E-01
2.00E-01
0.00E+00
-2.00E-01
[(myS)^2/Hz]
0
20
40
60
80
100
120
[Hz]
B3a
B3b
B3c

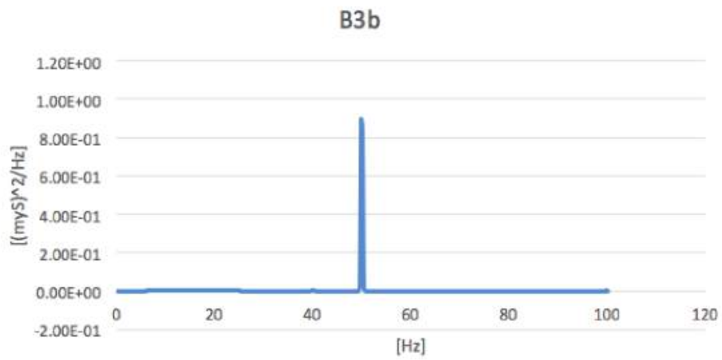

B3b
1.20E+00
1.00E+00
8.00E-01
6.00E-01
4.00E-01
2.00E-01
0.00E+00
-2.00E-01
[(myS)^2/Hz]
0
20
40
60
80
100
120
[Hz]

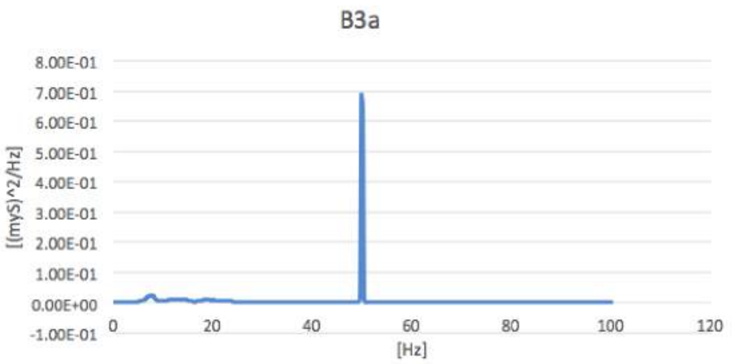

B3a
8.00E-01
7.00E-01
6.00E-01
5.00E-01
4.00E-01
3.00E-01
2.00E-01
1.00E-01
0.00E+00
-1.00E-01
[(myS)^2/Hz]
0
20
40
60
80
100
120
[Hz]

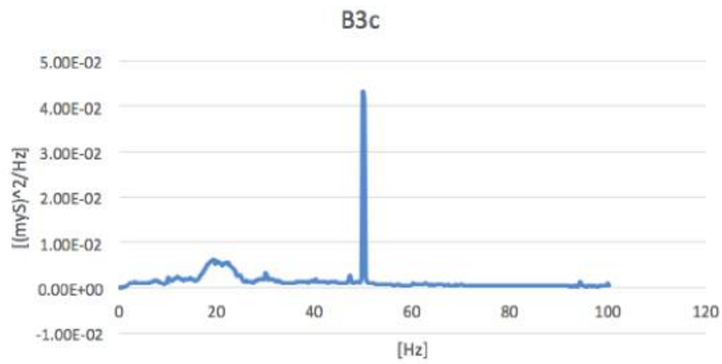

B3c
5.00E-02
4.00E-02
3.00E-02
2.00E-02
1.00E-02
0.00E+00
-1.00E-02
[(myS)^2/Hz]
0
20
40
60
80
100
120
[Hz]

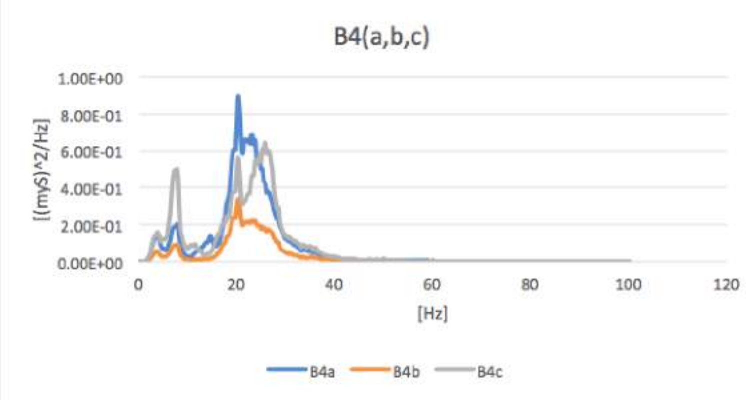
B4(a,b,c)
[(myS)^2/Hz]
1.00E+00
8.00E-01
6.00E-01
4.00E-01
2.00E-01
0.00E+00
0
20
40
60
80
100
120
[Hz]
B4a
B4b
B4c

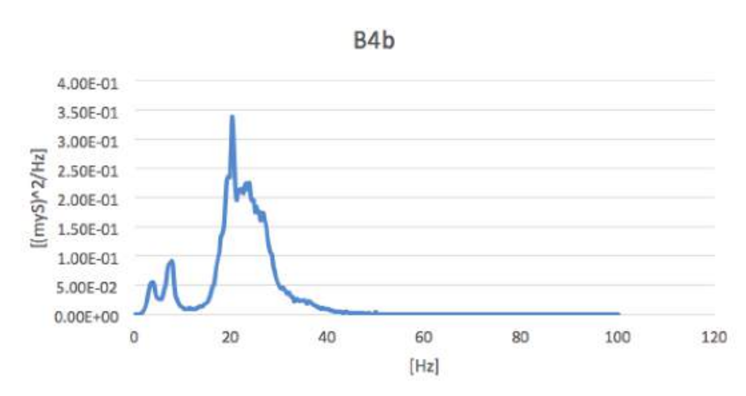
B4b
[(myS)^2/Hz]
4.00E-01
3.50E-01
3.00E-01
2.50E-01
2.00E-01
1.50E-01
1.00E-01
5.00E-02
0.00E+00
0
20
40
60
80
100
120
[Hz]

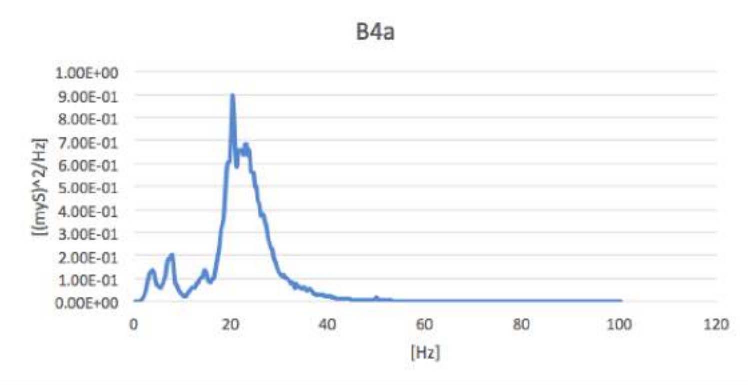
B4a
[(myS)^2/Hz]
1.00E+00
9.00E-01
8.00E-01
7.00E-01
6.00E-01
5.00E-01
4.00E-01
3.00E-01
2.00E-01
1.00E-01
0.00E+00
0
20
40
60
80
100
120
[Hz]

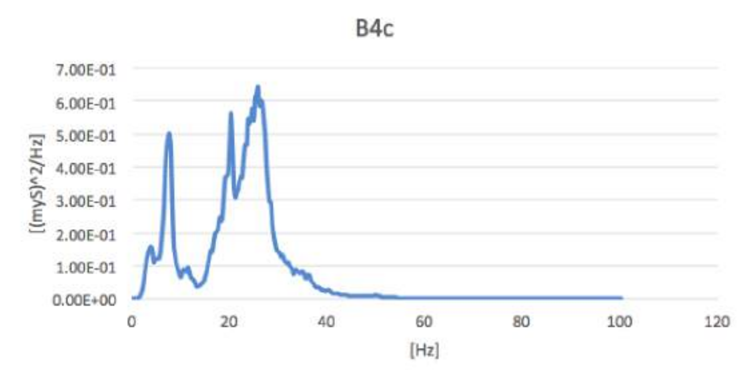
B4c
[(myS)^2/Hz]
7.00E-01
6.00E-01
5.00E-01
4.00E-01
3.00E-01
2.00E-01
1.00E-01
0.00E+00
0
20
40
60
80
100
120
[Hz]

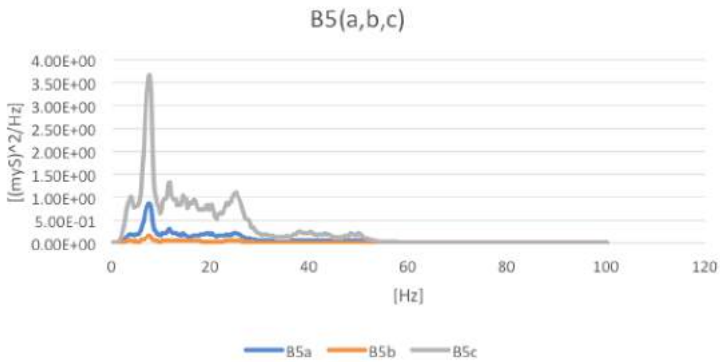
B5(a,b,c)
[(myS)^2/Hz]
4.00E+00
3.50E+00
3.00E+00
2.50E+00
2.00E+00
1.50E+00
1.00E+00
5.00E-01
0.00E+00
0
20
40
60
80
100
120
[Hz]
B5a
B5b
B5c

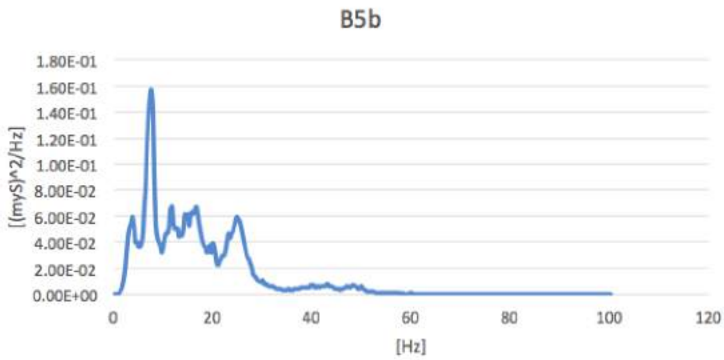
B5b
[(myS)^2/Hz]
1.80E-01
1.60E-01
1.40E-01
1.20E-01
1.00E-01
8.00E-02
6.00E-02
4.00E-02
2.00E-02
0.00E+00
0
20
40
60
80
100
120
[Hz]

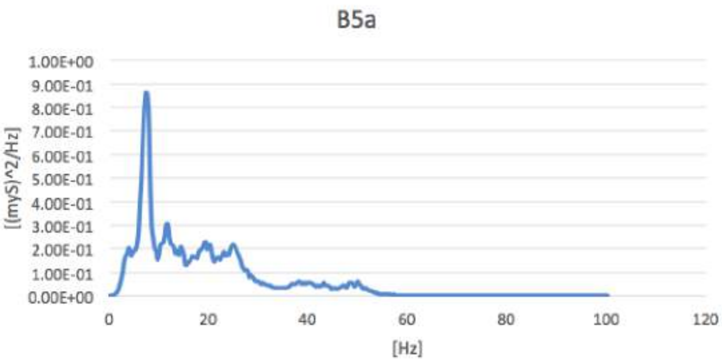
B5a
[(myS)^2/Hz]
1.00E+00
9.00E-01
8.00E-01
7.00E-01
6.00E-01
5.00E-01
4.00E-01
3.00E-01
2.00E-01
1.00E-01
0.00E+00
0
20
40
60
80
100
120
[Hz]

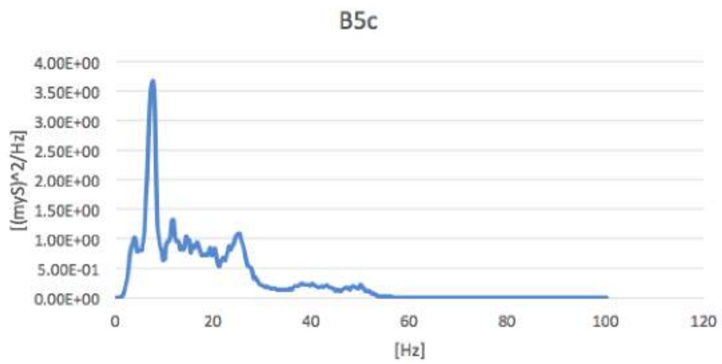
B5c
[(myS)^2/Hz]
4.00E+00
3.50E+00
3.00E+00
2.50E+00
2.00E+00
1.50E+00
1.00E+00
5.00E-01
0.00E+00
0
20
40
60
80
100
120
[Hz]

C

Appendix- ASTM D4169-16 DC3

ASTM D4169-16 Truck Vibration Changes *

ASTM D4169-**14** DC3

- 180 minutes divided amongst all possible shipping orientations
  - 60 minutes per axis
- Profile based on Assurance Level I, II, or III

-14 Version

Truck:			
	Power Spectral Density Level, g^2/Hz		
	Assurance Level	Assurance Level	Assurance Level
Frequency, Hz	I	II	III
1	0.0001	0.00005	0.000025
4	0.02	0.01	0.005
16	0.02	0.01	0.005
40	0.002	0.001	0.0005
80	0.002	0.001	0.0005
200	0.00002	0.00001	0.000005
Overall, g rms	0.73	0.52	0.37
Duration, min[B]	180	180	180

ASTM D4169-**16** DC3

- 180 minutes divided amongst all possible shipping orientations
  - Up to 3 axes
- All the following High, Medium, and Low level Truck profiles tested (no assurance levels)
  - Low Level: 120 minutes (40 minutes per axis)
  - Medium Level: 45 minutes (15 minutes per axis)
  - High level: 15 minutes (5 minutes per axis)

TABLE 2 TRUCK—Power Spectral Density Levels

Frequency	Power Spectral Density Level, G^2/Hz		
	High Level	Medium Level	Low Level
1	0.00072	0.00072	0.0004
3	0.030	0.018	0.010
4	0.030	0.018	0.010
6	0.0012	0.00072	0.00040
12	0.0012	0.00072	0.00040
16	0.0060	0.0036	0.0020
25	0.0060	0.0036	0.0020
30	0.0012	0.00072	0.00040
40	0.0060	0.0036	0.0020
80	0.0060	0.0036	0.0020
100	0.00060	0.00036	0.00020
200	0.000030	0.000018	0.000010
Overall G_{rms}	0.70	0.54	0.40

-16 Version

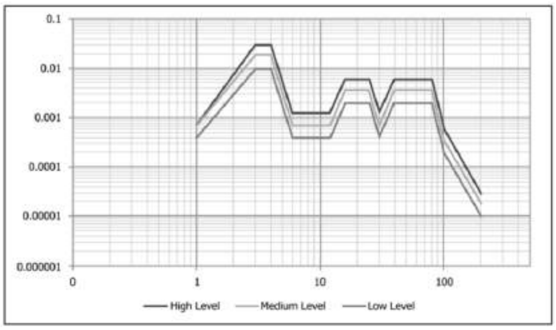

* NOTE: Only the TRUCK profile is affected; there are no changes to any other testing schedules.

ASTM D4169-16 Truck Vibration Changes *

ASTM D4169-**14** DC13

-14 Version

- 180 total minutes
  - 60 minutes truck
  - 120 minutes air
  - Divided amongst all possible shipping orientations
    - Truck: 20 min each base, side, end
    - Air: 40 min each base, side, end
- Profiles based on Assurance Level I, II, or III

Truck:

Frequency, Hz	Power Spectral Density Level, g^2/Hz Assurance Level I	Assurance Level II	Assurance Level III
1	0.0001	0.00005	0.000025
4	0.02	0.01	0.005
16	0.02	0.01	0.005
40	0.002	0.001	0.0005
80	0.002	0.001	0.0005
200	0.00002	0.00001	0.000005
Overall, g rms	0.73	0.52	0.37
Duration, min[B]	180	180	180

Air:

Frequency, Hz	Power Spectral Density Level, g^2/Hz Assurance Level I	Assurance Level II	Assurance Level III
2	0.0004	0.0002	0.0001
12	0.02	0.01	0.005
100	0.02	0.01	0.005
300	0.00002	0.00001	0.000005
Overall, g rms	1.49	1.05	0.74
Duration, min[B]	180	180	180

ASTM D4169-**16** DC 13

- 180 minutes divided amongst all possible shipping orientations
  - Up to 3 axes
    - 60 minutes truck
    - 120 minutes air
- All the following High, Medium, and Low level Truck profiles tested (No assurance levels)
  - Truck Low Level: 40 minutes (13 min, 20 sec per axis)
  - Truck Medium Level: 15 minutes (5 min per axis)
  - Truck High level: 5 minutes (1 min, 40 sec per axis)
- Air profile based on Assurance Level I, II, or III
  - 40 minutes per axis

TABLE 2 TRUCK—Power Spectral Density Levels

Frequency	Power Spectral Density Level, G^2/Hz High Level	Medium Level	Low Level
1	0.00072	0.00072	0.0004
3	0.030	0.018	0.010
4	0.030	0.018	0.010
6	0.0012	0.00072	0.00040
12	0.0012	0.00072	0.00040
16	0.0060	0.0036	0.0020
25	0.0060	0.0036	0.0020
30	0.0012	0.00072	0.00040
40	0.0060	0.0036	0.0020
80	0.0060	0.0036	0.0020
100	0.00060	0.00036	0.00020
200	0.000030	0.000018	0.000010
Overall G_{rms}	0.70	0.54	0.40

-16 Version

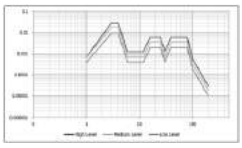

TABLE 4 AIR—Power Spectral Density Levels

Frequency	Power Spectral Density Level G^2/Hz Assurance Level I	II	III
2	0.0004	0.0002	0.0001
12	0.02	0.01	0.005
100	0.02	0.01	0.005
300	0.00002	0.00001	0.000005
Overall G_{rms}	1.49	1.05	0.74

* NOTE: Only the TRUCK profile is affected; there are no changes to any other testing schedules.

D

Appendix- Calculations

Hanging of Windscreen - Trigonometry

Angle Placement of Windscreen for Modal Analysis
Height of windscreen: 908 mm
Angle Placement in Car: 33 degrees

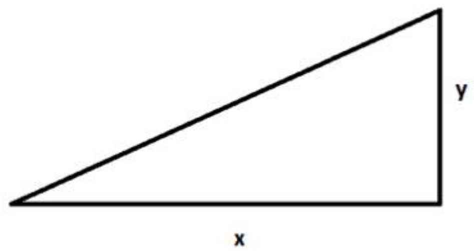

Nominal Sampling Interval - Nyquist Equation
Speed of sound in glass: 4540 m/s
Sampling frequency: 200 Hz

$$f_s = 2 * 200 = 400 \tag{D.1}$$

$$\lambda = 4540/400 = 11,35m \tag{D.2}$$

Boundary Condition windscreen load - Static Mechanics (Force Vector)
Quantity: 1 (for this demonstration)
Acceleration of Gravity: g
Mass: m
Angle: v
Length: l

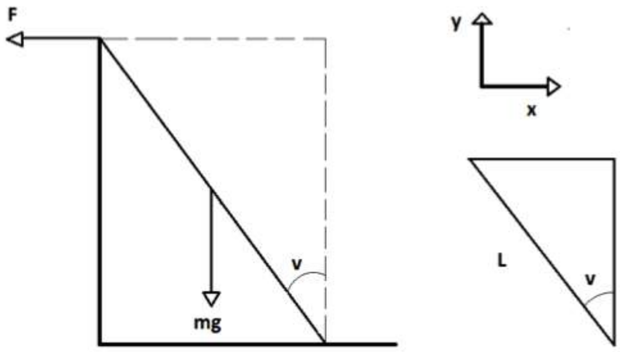

$$F_x = (1 * -m * g) * l * \sin(v) \tag{D.3}$$

$$F_y = (1 * -m * g) * l * -\cos(v) \tag{D.4}$$

E

Appendix- Material Properties - ANSA Input

Material Property -Glass

Material Property -PVB